School of Earth and Ocean Sciences
University of Victoria
P.O. Box 3055 STN CSC
Victoria, BC Canada V8W 3P6

Results from an acoustic modelling study of seismic airgun survey noise in Queen Charlotte Basin

by Alexander O. MacGillivray[1] and N. Ross Chapman[2]

1 Current address: JASCO Research Ltd., Victoria BC
2 School of Earth and Ocean Sciences, University of Victoria

December 7, 2005

Table of Contents

List of Tables

List of Figures

Executive Summary

This report details the methods and describes the results of an acoustic modelling study that addresses the issue of seismic survey noise propagation in the Queen Charlotte Basin (QCB). The goal of this study is to provide information to fill the knowledge gap regarding the physical aspects of sound transmission in QCB. This information is vital for any studies that consider the potential effects of anthropogenic sound may have on marine mammals and fish. This study applies modern acoustic propagation modelling techniques, using up-to-date data on the ocean environment as model input parameters, to forecast noise levels from typical seismic exploration sources in the QCB.

The potential effects of airgun noise on marine mammals and fish are both physiological and behavioural: within a few hundred metres of an array, airgun noise may induce a shift in hearing threshold; at longer ranges, airgun noise may displace individual animals or mask calls between individuals. The noise level to which an animal is exposed depends both on the loudness of the seismic source and the losses that occur in transmission of energy from that source to the organism in question. The current study addresses the physical aspects of sound transmission — *i.e.*, the sound generation at the source and acoustic transmission loss problems — for an airgun survey in the QCB.

The scope of this study can be summarized as follows:

- To numerically simulate underwater sound transmission in Queen Charlotte Basin in areas where exploration activities are likely to be conducted.
- To forecast received noise levels by combining acoustic transmission loss computations with acoustic source levels representative of seismic exploration activity.
- To use received level forecasts to estimate zones of impact for marine mammals.

The Queen Charlotte Basin is characterized by shallow water, complex bathymetry, and a highly variable sound speed profile. In such an environment, acoustic transmission depends particularly on the interaction of the sound field with the ocean bottom and simple empirical sound spreading laws do not provide accurate predictions of the sound field at distant ranges from the noise source. However, given a sufficient amount of knowledge about the ocean environment, one can accurately model acoustic transmission loss using a computer-based acoustic modelling code. The critical environmental parameters are the bathymetry of the ocean, the sound speed profile in the water, and the geoacoustic profile of the seabed and subbottom. Databases for all these model parameters are generated from existing sources.

The current study uses the RAM acoustic propagation model for computing acoustic transmission loss in the QCB. RAM, which was developed by the US Naval Research Laboratory, has been extensively benchmarked for accuracy and is widely employed in the underwater acoustics community. A full-waveform airgun array source signature model is used to accurately compute the source level and directionality of the seismic array. Source level predictions from the airgun model are combined with acoustic

transmission loss computed by RAM to provide sound levels for single airgun pulses over the entire extent of the basin.

In addition to the sound level predictions, this study presents a methodology for modelling noise propagation from seismic surveys in the QCB. Seismic source locations are positioned along survey track lines that traverse zones in the basin with high potential for oil and gas deposits. Maps of received noise levels are presented for nine different source scenarios at positions along two survey tracks. Several key findings of this noise modelling study are:

- Received noise levels in the water are influenced by the source location, array orientation and the shape of the sound speed profile with respect to water depth.
- Received noise levels are lowest in those areas of the basin with shallow bathymetry (*e.g.*, Dogfish Banks) due to scattering and absorption of sound at the seabed.
- In contrast, surface-duct propagation conditions in deeper water result in the highest received levels at long ranges.
- The effect of the sound speed profile on received levels increases significantly with range from the source, with differences greater than 20 dB observed beyond 100 km, between down-refracting and surface-duct propagation conditions.
- Mean ranges to the 170 dB sound level contour (approximately equivalent to NMFS 180 dB 90% RMS threshold level) vary from 0.54 km to 1.15 km. The range to the 170 dB contour is greater in shallower water than in deeper water.
- The highest levels from the airgun array are in the broadside direction, which is the direction of maximum energy transmission from the array.

The methodology developed in this project can be applied to other QCB seismic survey scenarios as required.

Acknowledgements

This report was completed by Alex MacGillivray as part of a Master's Thesis project jointly sponsored by JASCO Research Ltd. and the University of Victoria under the NSERC Industrial Post-graduate Scholarship (IPS) program. The authors would like to thank the following individuals for their assistance and expertise, which contributed to the success of this study:

- Terry Curran, of the Canadian Hydrographic Service, for amassing and providing the high-resolution bathymetry dataset for QCB.
- Dr. Bill Crawford and Dr. Frank Whitney, of the Institute of Ocean Sciences, for providing the oceanographic temperature/salinity dataset for QCB.
- Dr. Vaughn Barrie, of the Pacific Geoscience Centre, for providing access to Huntec survey records for QCB.
- Dr. Kristin Rohr, of Rohr Consulting, for suggesting probable locations and times for oil & gas exploration in QCB.
- Julie Halliday, of the UVic School of Earth and Ocean Sciences, for providing sediment thickness maps for a section of Moresby trough.

Several other people lent their help and/or expertise to the authors of this study: Dr. Roslyn Canessa and Roger Stephen of the UVic Geography Dept., Brendan Mather of the BC Ministry of Energy and Mines, Steve Glavin of Nautical Data Intl., Dr. Chris Tindle of the University of Auckland and W. John Richardson, Bob Bocking and Mike Demarchi of LGL Ltd.

1. Introduction

In recent years there has been renewed interest in opening the British Columbia offshore region to oil and gas exploration and development. This interest comes in light of new scientific research indicating that there may be significant oil and gas deposits, larger than previously expected, in the sedimentary basins located off the coast of BC. Particular attention has focused on the Queen Charlotte Basin (QCB) where the largest oil and has deposits are believed likely to be located [Hannigan *et al.*, 2001]. A recent expert panel report by the Royal Society of Canada advises that many science gaps exist with regards to the potential impact of hydrocarbon exploration and development in the BC offshore region [RSC 2004].

One consequence of opening the QCB to oil and gas exploration is that marine mammals and fish will be exposed to heightened levels of underwater noise, in particular from periodic seismic airgun activity. The QCB is an important habitat for several threatened and endangered species of marine mammals and fish [RSC 2004, Tab. 5.1]. The potential effects of airgun noise on marine mammals and fish are both physiological and behavioural: within a few hundred metres of an array, airgun noise may induce a temporary shift in hearing threshold; at longer ranges airgun noise may displace individual animals or mask calls from conspecifics [Richardson *et al.* 1995 §10.1]. A necessary first step in assessing seismic exploration's potential impact on marine mammals and fish in QCB is to estimate the extent to which seismic oil and gas survey activities are likely to the ensonify the waters of this coastal region.

This report details the methods and describes the results of an acoustic modelling study that has been carried out to address the issue of seismic survey noise propagation in the QCB. The noise field generated by a seismic airgun survey depends on both the loudness of the seismic source and the attenuation of sound due to propagation through the marine environment. In addition, the distribution of the noise field changes in time, as the seismic vessel advances along its survey track. Thus, the noise level to which a marine mammal or fish is exposed depends on the location of the survey vessel, its proximity to the airgun array and on the size of the airgun array. This report presents modelled noise levels from a representative seismic airgun survey in the QCB, for several probable survey locations. It is expected that noise level predictions from this study will facilitate an accurate and objective assessment of the potential impacts of seismic survey noise on marine mammals and fish in the QCB.

2. Scope

The goal of this study has been to help fill in the knowledge gap regarding the propagation of seismic survey noise in the QCB, so that the potential affect on marine mammals and fish can be assessed objectively. Until now, the acoustic transmission of seismic survey noise has not been studied on a basin scale in this region. This study has addressed this knowledge gap by applying modern acoustic propagation modelling techniques, using up–to–date data on the ocean environment, to forecast noise levels from a typical seismic exploration source in the QCB.

The scope of this study may be summarized as follows:

- To numerically simulate underwater sound transmission in Queen Charlotte Basin in areas where exploration activities are likely to be conducted.
- To forecast received noise levels by combining acoustic transmission loss computations with acoustic source levels representative of seismic exploration activity.
- To use received level forecasts to estimate zones of impact for marine mammals.

3. Background

3.1. Marine seismic surveys

Modern marine seismic airgun surveys are capable of high-resolution three-dimensional imaging of the earth's crust, down to several kilometres depth, and have thus become an essential tool both for the oil and gas industry and for research scientists studying the earth's structure and associated geological hazards (*e.g.*, earthquakes). Seismic airgun surveys are employed during the oil and gas exploration phase to locate potential hydrocarbon deposits and during the production phase to monitor the status of existing reservoirs. A typical airgun survey may last several months, the time to complete a survey depending on the size of the oil gas field that is being surveyed. Survey activity is generally confined to calm-weather months, an important consideration in an extreme environment such as QCB, since costly survey equipment is susceptible to damage in high seas and seismic data are very sensitive to noise induced by surface wave motion.

Seismic airgun surveys may be divided into two types, 2-D and 3-D, according to the type of data that they acquire. 2-D surveys are so-called because they only provide a two-dimensional cross-sectional image of the earth structure and are characterized by large spacing between survey lines, on the order of a kilometre or more. 3-D surveys, on the other hand, employ very dense line spacing, of the order of a few hundred metres, to provide a three-dimensional volumetric image of the earth structure. 3-D surveys are much more costly than 2-D surveys, since they cover less area in an equivalent time and require that a greater number of airguns and streamer cables be deployed. However, 3-D surveys are increasingly favoured by industry because they provide much higher quality data than 2-D surveys.

A typical airgun survey, either 2-D or 3-D, is operated from a single survey ship that tows both the seismic source and receiver apparatus. The seismic source is an airgun array consisting of many individual airguns that are fired simultaneously in order to generate a seismic pulse. In some cases, large surveys will employ more than one source array in order to increase the firing rate or the survey resolution; in this case the arrays will have nearly identical layouts and are fired in alternation. The receiver equipment consists of one or more streamer cables, several kilometres in length, that contain hundreds of sensitive hydrophones for detecting echoes of the seismic pulse reflected from sub-bottom features. As well, the survey ship will usually employ several smaller support vessels for deploying and retrieving cable, maintaining the streamers, monitoring for shallow hazards and notifying other vessels that happen to be in the survey path.

3.2. Airgun arrays

Large arrays of airguns, as typically employed by industry for seismic surveys, are broadband acoustic sources that project energy over a wide range of frequencies, from under 10 Hz to over 5 kHz. However, airgun arrays are designed to produce most of their energy below 200 Hz at frequencies useful for seismic profiling. Most of the underwater noise generated by a seismic survey is due to the airgun array; in comparison, the survey vessel itself and the support ships contribute very little to the overall noise field. The arrays consist of many airguns that are configured in such a way as to project the maximum amount of seismic energy vertically into the earth. However, much of the sound energy still leaks off to the sides of an array and into the surrounding environment.

The particular configuration of an airgun array depends on factors such as the survey type, desired penetration depth and the stock of available guns. The volumes and positioning of individual guns in an array are selected in such a way as to generate as clean a seismic pulse as possible — that is, as sharply peaked as possible with very little ringing in the vertical direction. Since the configuration of airgun arrays can be quite variable, they are usually described in terms of their total volume (i.e., the sum of the volumes of the guns comprising the array). The total volume of an airgun array employed in an oil and gas survey will typically be several thousand cubic inches and, as a rule of thumb, the loudness of an array is generally proportional to its volume, though there are exceptions to this rule for unusual array configurations.

Quoted (peak) source levels for airgun arrays are often as high as 255 dB re μPa at 1 metre. However, this apparently high value for the source level can lead to erroneous conclusions about the impact on marine mammals and fish for the following reasons:

1. Peak source levels for seismic survey sources are quoted relative to the vertical direction; however, due to the intrinsic directivity of the radiated sound field, source levels off to the sides of the array are generally much lower.
2. Far field source levels do not apply in the near field of the array where the individual airguns do not add coherently; sound levels in the near field are, in fact, lower than would be expected from far field estimates.

The source level of a seismic airgun array varies considerably in both the horizontal and vertical directions, due to the complex configuration of guns comprising the array. Thus, one must account for this variability in order to correctly predict the sound field generated by an airgun array. In practice it is extremely difficult, and often impractical, to measure the source level of a large airgun array *in situ*. However, if the source signatures of the individual airguns are known, then it is possible to accurately compute the source level of an array by summing up the contributions of the array elements with the appropriate phase delays corresponding to their relative positions. This latter approach is most often used to determine the source level of an airgun array and has been shown to be quite accurate [Ziolkowski *et al.*, 1982].

3.3. Acoustic propagation modelling

Water transmits sound far better than other kinds of radiation, including light, which is why so many marine organisms rely on their hearing to find prey, avoid predators, and to communicate. This is also the reason why acoustic sources, such as sonar and airguns,

are useful for mapping the ocean and for studying the sub-bottom. However, underwater sound propagation is a complex phenomenon, and simple spherical spreading laws for sound intensity do not provide an accurate description of the sound field in the ocean. This is because interactions at the ocean surface and bottom reflect sound back into the water column, and refraction, caused by small vertical variations in the sound speed, can bend sound rays and carry them to great distances. In general, one requires a wave-theory model, which solves the physical equations governing acoustic propagation in the ocean, to accurately model sound transmission.

Ocean acoustic propagation models may be divided into four classes, based on the technique that is used to solve the wave equation: ray theory, normal modes, wave-number integral and parabolic equation. Each class of model employs a different set of approximations to render the solution of the wave equation tractable. Thus, each class of model is applicable under different circumstances. The current study has employed the acoustic propagation model RAM [Collins, 1993], which is based on the parabolic equation solution to the acoustic wave equation (see §4.2). Parabolic equation models solve an approximate "one-way" wave equation that neglects back-scattered sound energy and are the most efficient class of model for low frequency problems in range-dependent environments such as QCB. The RAM model has been extensively benchmarked against exact solutions of the wave equation, is highly accurate, and has been used for a wide variety of ocean acoustic applications.

Acoustic propagation models usually compute the pressure field generated by an omnidirectional point source of unit power. Converted to decibel units, this is equivalent to *transmission loss* — the attenuation of sound pressure due to propagation through the environment. The advantage of this approach is that the received sound level, *RL*, may be computed by simply subtracting the transmission loss, *TL*, from the source level, *SL*:

$$RL = SL - TL \tag{1}$$

Note that these quantities are expressed in decibel units, and are functions of position, frequency and beam angle. In this way, the acoustic transmission loss may be modelled separately from the source, since the transmission loss and source level are assumed to be independent.

The accuracy of the sound field predicted by an acoustic propagation model is limited by the quality and resolution of the available environmental data. There are three basic kinds of environmental data that affect sound propagation in the ocean, and are required as input into an acoustic propagation model:

1. bathymetry data of the ocean depth;
2. sound speed profiles in the ocean;
3. geoacoustic profiles of the ocean subbottom.

Accurate bathymetry data are especially important in shallow water, where acoustic propagation is strongly influenced by interaction of sound with the sea bottom. Variations in the depth and slope of the bottom cause sound energy to be scattered and absorbed by the seabed. The ability of a propagation model to accurately reproduce features of the sound field in shallow water depends on the resolution of the available

bathymetry data. Digital bathymetry data may typically be obtained from existing water depth databases and from hydrographic charts.

The sound speed profile in the ocean can strongly influence long-range acoustic propagation by refracting and trapping sound energy in the water column. The speed of sound in seawater is a function of temperature, salinity and depth. However, temperature and salinity are not static, and changes occur on diurnal and seasonal time scales due to oceanographic mixing and transport processes. These changes in temperature and salinity affect the sound speed profile. Representative sound speed profiles for a particular region may be determined by reviewing historical temperature/salinity profiles. The variability in the transmission loss, due to the changes in the sound speed profile, may be bracketed by calculating the transmission loss for 'limiting case' profile shapes.

Geoacoustic properties of the ocean bottom materials, which include the compressional speed, shear speed, density and attenuation, govern the degree to which sound is reflected and absorbed at the seabed. However, these are often the most difficult type of environmental data to obtain. Geoacoustic profiles — *i.e.*, profiles of geoacoustic parameters versus seabed depth — may be measured directly from sediment cores, but cores are costly to obtain and to analyze and so the availability of this kind of data is limited. Most often, geoacoustic profiles must be inferred from a combination of historical seismic data and knowledge of the local geology.

3.4. Sound level metrics

3.4.1. Broadband metrics

Sound pressure underwater is measured in decibels relative to a fixed reference pressure of 1 μPa. However there are several different metrics of sound pressure (*i.e.*, ways of measuring sound pressure) that are found in the literature. The three most common for impulsive sounds are peak pressure level, sound pressure level and sound exposure level. It is very important to be aware which metric has been quoted when comparing measurements from different studies, since the difference between the various metrics may be as large as 20 dB.

The peak sound pressure level (symbol L_{pk}) is the maximum instantaneous sound pressure level attained by a signal, $p(t)$ [ANSI S1.1 1984 3.52, 4.13]:

$$L_{pk} = 20\log_{10}\left(\max\left|p(t)\right|\right) \qquad (2)$$

This metric is very commonly quoted for impulsive sounds but does not take into account the pulse duration or bandwidth of a signal. Furthermore, the peak pressure is difficult to model accurately at any great distance from the source using standard broadband modelling techniques.

The sound pressure level or SPL (symbol L_p) is the decibel level of the mean square pressure over some fixed time window, T [ANSI S1.1 1984 3.53, 4.08]:

$$L_p = 10\log_{10}\left(\frac{1}{T}\int_T p^2(t)\,dt\right) \qquad (3)$$

In general, this is a better metric than the peak pressure for use in impact studies and is often encountered in the literature. However, a subtle issue involved in applying this metric to impulsive sounds is the selection of a standard averaging window over which to compute the mean square pressure. Thus, when quoting sound pressure level, it is very important to be aware of the length of integration time window that has been used. For the current study sound pressure levels have been computed using an equivalent 1 second averaging time window.

In studies of impulsive noise, the sound pressure level is often computed over the "pulse duration", rather than over a fixed time window. In this case, the SPL is usually defined so that the time window, T_{90}, is taken to be the interval containing 90% of the pulse energy — commonly referred to at the 90% RMS SPL (L_{p90}). Unfortunately, this metric is only suitable for *in situ* measurement, since the variable time window implicit in the definition of the 90% RMS SPL is nearly impossible to model accurately. As well, the 90% RMS metric itself has no special biological significance with regards to the hearing of marine mammals or fish. Thus, the 90% RMS SPL values are *not* quoted in the current study, nor would it be feasible to do so.

The sound exposure level or SEL (symbol L_E) is the time-integral of the square pressure over a fixed time window [ANSI S1.1 1984 3.54, 4.21]:

$$L_E = 10\log_{10}\left(\int_T p^2(t)\,dt\right) \qquad (4)$$

For impulsive events, the time window is usually taken to be 1 second in length from the onset of the pulse. Strictly speaking, this metric has units of μPa·√s rather than μPa and is not actually a measure of sound pressure but of sound energy[1]. Nonetheless, this metric is closely related to the sound pressure level since the two are computed in a very similar fashion. In fact, SEL and SPL are equivalent if the integration time window, T, for both metrics is chosen to be 1 second. However, unlike the sound pressure level, the sound exposure level is applied as a dosage metric, meaning that its value increases with the number of exposure events. Due to the lack of ambiguity in its definition, the sound exposure level is increasingly being used in noise exposure studies. In addition, the sound exposure level may be modelled quite accurately, under most conditions, using standard acoustic models.

Received level values quoted in this report are given in terms of sound exposure level (SEL) for a single airgun pulse, or equivalently, in terms of sound pressure level (SPL) over a 1-second averaging window.

[1] Sound exposure is also referred to as energy flux density (EFD) in the literature. However, strictly speaking, the integral of squared sound pressure is only equal to the energy flux density for plane waves.

One difficulty with using SEL is that much of the literature regarding the impact of anthropogenic noise on marine mammals and fish quotes measured sound levels in terms of SPL over the pulse duration. For example, the current US National Marine Fisheries Service guidelines regarding marine mammals and seismic noise are cast in terms of the 90% RMS level (see §7.1). Fortunately, if the pulse duration, T_{90}, is known (or may be estimated) then the SEL may be computed from the 90% RMS level via a simple relation:

$$L_E = L_{p90} + 10\log(T_{90}) + 0.458 \qquad (5)$$

where the last term accounts for the fact that only 90% of the acoustic pulse energy is delivered over the standard integration period.

3.4.2. Frequency domain metrics

It is important to take into account the frequency distribution of anthropogenic noise when considering its potential impact on marine mammals and fish, since the effect of noise will be significantly diminished if it falls outside the hearing range the organism in question. A convenient way of expressing the frequency content of a broadband signal is in terms of 1/3-octave band pressure levels (symbol L_b). In 1/3-octave band analysis, sound is band-pass filtered into several adjacent frequency bins, and the mean-square pressure level in each bin is computed. The resultant 1/3-octave band levels give the frequency distribution of sound energy within the signal. The acoustics community has adopted standard 1/3-octave frequencies in order to facilitate comparisons between studies; the centre frequencies of these standard pass-bands are shown in Table 1.

Band pressure levels possess the convenient property that, when the power in all bands is summed together, it equals the total sound pressure level of the broadband signal:

$$L_p = 10\log_{10}\sum_n 10^{L_{bi}/10} \qquad (6)$$

where L_{bi} is the band pressure level in band i. Thus, for broadband signals, acoustic transmission loss is very often modelled in 1/3-octave bands. The advantage of 1/3-octave band modelling is that it can resolve the frequency dependent propagation characteristics of a particular environment and still be used to efficiently compute the overall sound pressure level for any receiver position.

Table 1: List of standard 1/3-octave band centre frequencies, in units of Hz, over four decades. For the current study, acoustic transmission loss was modelled in 1/3-octave bands from 8 Hz to 1000 Hz (indicated by bold face type).

Band Centre Frequency f_c (Hz)			
1	**10**	**100**	**1000**
1.3	**12.5**	**125**	1250
1.6	**16**	**160**	1600
2	**20**	**200**	2000
2.5	**25**	**250**	2500
3.2	**31.5**	**315**	3150
4	**40**	**400**	4000
5	**50**	**500**	5000
6.3	**63**	**630**	6300
8	**80**	**800**	8000

4. Methods

4.1. Airgun array source model

The current study employs a full-waveform airgun array source signature model in order to accurately compute the source level and directionality of a seismic array. The source signature model, which is implemented in Fortran, numerically simulates the oscillation and radiation of airgun bubbles. The theory of the source model is beyond the scope of this report but is based on the pioneering work of Ziolkowski [1970] who first modelled the pressure waveforms of seismic airguns. In addition to the basic bubble physics, the source model also accounts for non-linear pressure interactions between airguns, port throttling, and bubble damping. The source model includes four empirical parameters that are tuned so that the model output matches observed airgun behaviour; these parameters are similar to those employed by authors such as Dragoset [1984] and Landro [1990]. The model parameters were fit to a large library of real airgun data using a "simulated annealing" global optimization algorithm. These airgun data were obtained from a previous study [Racca & Scrimger, 1986] that measured the signatures of Bolt 600/B guns ranging in volume from 5 in^3 to 185 in^3. The airgun array source model requires several inputs, including the array layout, airgun volumes, and firing pressure. The output of the source model is a set of "notional" signatures for the array elements. The notional signatures are the pressure waveforms of the individual airguns, in the absence of the other array elements, at a standard reference distance of 1 metre.

After the source model is executed, the resulting notional signatures are summed together with the appropriate phase delays to obtain the far-field source signature of the array. The far-field array signature, in turn, is filtered into 1/3-octave pass bands to compute the source level of the array as a function of frequency band, f_c, and propagation azimuth, θ:

$$SL = SL(f_c, \theta) \tag{7}$$

Though straightforward, the mathematical details of computing the far-field source level are too involved to be discussed here and are instead provided in Appendix A.

For the acoustic modelling, an airgun array was constructed that was representative of the typical sort of array geometries employed by industry for oil and gas surveying. The layout of the array is shown in Figure 1. This particular array is a medium size airgun array, with a total volume of 3000 in^3, consisting of 32 guns in four strings and towed at a depth of 6 metres. The far-field signature of the array, in both the vertical and broadside directions, is shown in Figure 2. The directionality patterns of the airgun array, in 1/3-octave frequency bands, are presented in Appendix B.

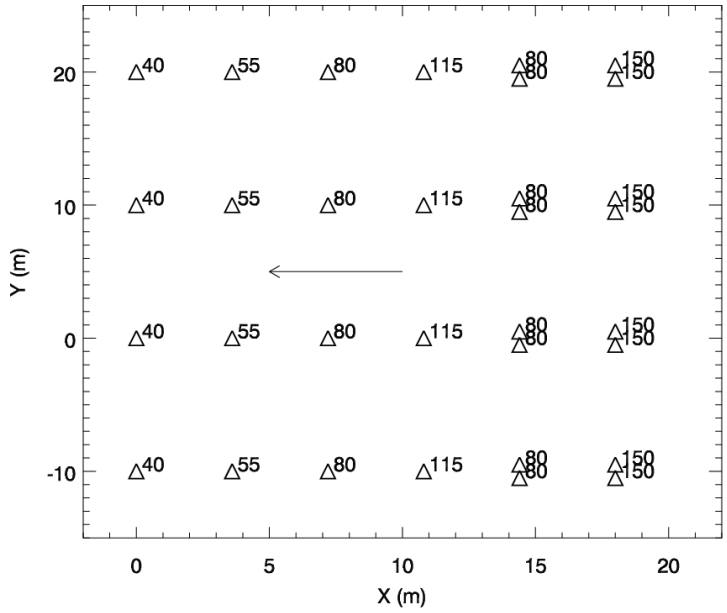

Figure 1: Plan view diagram of the airgun array employed for the current modelling study (total volume 3000 in^3). The volumes of individual guns are given in units of cubic inches. The arrow indicates the tow direction of the array.

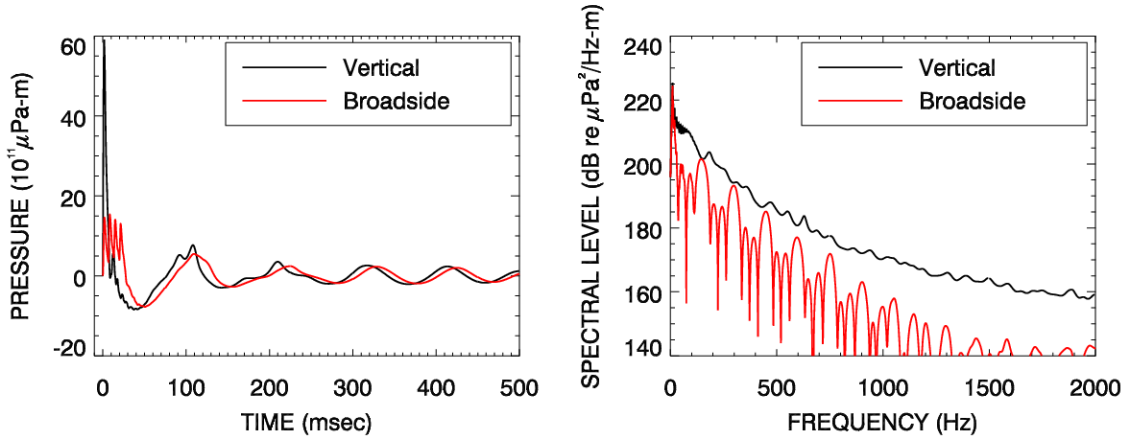

Figure 2: (Left) Modelled far-field signature of the airgun array in both the vertical and horizontal (broadside) directions. (Right) Spectra showing the frequency distribution of acoustic energy in the seismic signal.

The propagation model, RAM, calculates transmission loss for an equivalent point-like acoustic source. However, an airgun array consists of many sources and so the point-source assumption is not valid in the near field, where the array elements do not add coherently. The distance to the near field of an array is given by the expression:

$$R_{nf} < \frac{L^2}{4\lambda} \qquad (8)$$

where λ is the sound wavelength and L is the longest dimension of the array [Lurton, 2002, §5.2.4]. Along the diagonal of the airgun array of Figure 1, $L \approx 36$ metres and so the maximum near field range is 216 metres at 1 kHz (R_{nf} is less for lower frequencies). Beyond this range it is assumed that an array radiates like a point source and can be treated as such for the purpose of propagation modelling.

4.2. Transmission loss model

The Queen Charlotte Basin is characterized by shallow water, complex bathymetry, and a highly variable sound speed profile. In such an environment, acoustic transmission is particularly dependent on the interaction of the sound field with the ocean bottom and simple empirical sound spreading laws do not apply. However, given a sufficient amount of knowledge of the physical environment, it is possible to accurately model acoustic transmission loss using a computer-based acoustic modelling code.

The current study uses RAM — the Range-dependent Acoustic Model, developed by M. Collins at the Naval Research Laboratory — for computing acoustic transmission loss in the QCB. RAM, which is implemented in Fortran, is based on the parabolic equation (PE) solution to the acoustic wave equation and is widely used in the ocean acoustics community because it has proven highly accurate and efficient. RAM correctly solves range-dependent ocean acoustics problems with arbitrary bottom layering and, unlike some other PE based modelling codes, RAM accounts for steep propagation angles by using a wide-angle, Padé series expansion of the PE operator. The theory behind RAM, which is discussed in detail in Collins' 1993 article, is beyond the scope of this report.

The particular RAM variant that was employed in the current study is RAMGEO, derived from version 1.5 of the RAM source code. RAMGEO implements a stratified seabed model in which multiple bottom layers run parallel to the bathymetry. To account for losses due to shear wave conversion in elastic media, which can be an important sound absorption mechanism in shallow water environments, RAMGEO was modified to use a complex-density equivalent fluid bottom approximation [Zhang & Tindle, 1995]. The equivalent fluid approximation treats an elastic material as a fluid with a complex-valued density. The small imaginary component of the bottom density absorbs acoustic energy at certain incidence angles, thus simulating the conversion of sound waves in the water to elastic shear waves in the bottom. Although this approximation is only valid for low shear speeds ($c_s < 600$ m/s) it allows for significantly faster computations than a fully elastic bottom model.

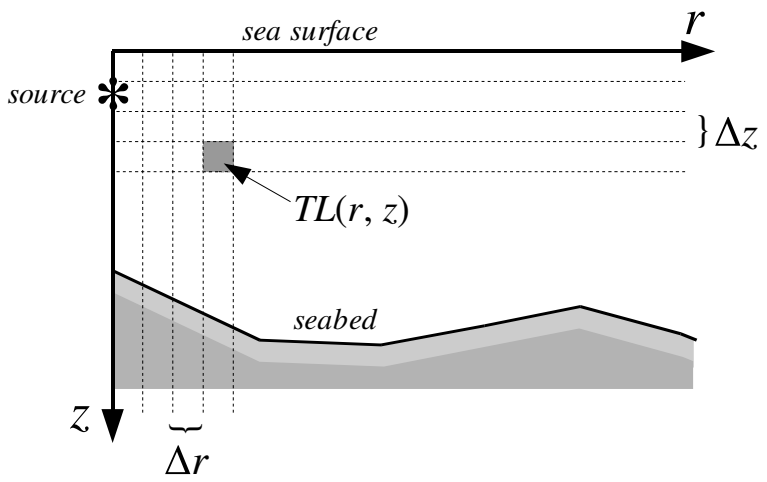

Figure 3: Diagram of the range/depth grid on which RAM computes acoustic transmission loss, *TL*(*r*, *z*).

Table 2: List of RAM modelling grid resolutions and vertical grid sizes used in each 1/3-octave frequency band.

f_c (Hz)	Δr (m)	Δz (m)	z_{max} (m)	f_c (Hz)	Δr (m)	Δz (m)	z_{max} (m)
8	50	2.5	1200	100	50	0.5	700
10	50	2.5	1000	125	50	0.5	700
12.5	50	1.25	900	160	50	0.5	700
16	50	1.25	900	200	25	0.25	700
20	50	1.25	900	250	25	0.25	700
25	50	1.25	800	315	25	0.25	700
31.5	50	1.25	800	400	20	0.25	700
40	50	1.0	800	500	10	0.125	700
50	50	1.0	700	630	10	0.125	700
63	50	1.0	700	800	10	0.125	700
80	50	1.0	700	1000	10	0.125	700

RAM computes acoustic transmission loss on a two-dimensional range/depth grid that extends radially outward from the source position, as shown in Figure 3. At each range step along the grid, the bathymetry, sound speed profile and geoacoustic profile of the environment are specified. Since RAM uses a finite-difference solver, the convergence of the solution depends on the range and depth resolution of the computation grid, Δr and Δz. Appropriate values for Δr and Δz were determined for the QCB environment by performing a battery of convergence tests along representative radials, in 1/3-octave bands. Table 2 shows the modelling grid resolutions that were used in the current study, as well as the maximum vertical extent of the grid, for each frequency band.

To model the acoustic field in three-dimensions, RAM was run along many closely spaced radials, centred about the source position. This technique, known as N×2-D modelling, neglects the scattering of acoustic energy between radials. A fully three-dimensional acoustic model, on the other hand, would be capable of accounting for acoustic scattering between radials but is an order of magnitude slower than an equivalent N×2-D model. Thus, given the available time and computing resources, a fully three-dimensional acoustic model could not be applied for the current study. However, the

N×2-D result is expected to be sufficiently accurately in most regions of the QCB since the transversely scattered component of the acoustic field is usually quite small.

For each source position, RAM was run at 22 frequencies along 144 constantly spaced radials covering a full 360º of azimuth. Transmission loss was computed in 1/3-octave bands from 8 Hz to 1 kHz — this frequency range contains the large majority of acoustic energy radiated by an airgun array. Thus, the transmission loss grids output by the model were functions of four dimensions:

$$TL = TL(r, z, \theta, f_c) \tag{9}$$

where r is range, z is depth, θ is the azimuth angle and f_c is band frequency. Since each model run generated a very large volume of transmission loss data, the output grids were subsampled to a constant resolution of 100 metres in range and 5 metres in depth, and transmission loss data below the seafloor were discarded. Even with this grid decimation applied, each model run generated approximately 500 MB of transmission loss data.

4.3. Physical environment databases

4.3.1. Bathymetry

For this study, high-resolution digital point bathymetry data were obtained from the Canadian Hydrographical Service for Dixon Entrance, Hecate Strait and Queen Charlotte Sound. The point bathymetry data, which cover the entire Queen Charlotte Basin, were projected into UTM x/y coordinates and were resampled onto a constant 100×100 metre grid using bilinear interpolation. Depth points along each modelling radial were taken from this bathymetry grid. Figure 4 shows a contour plot of the QCB bathymetry.

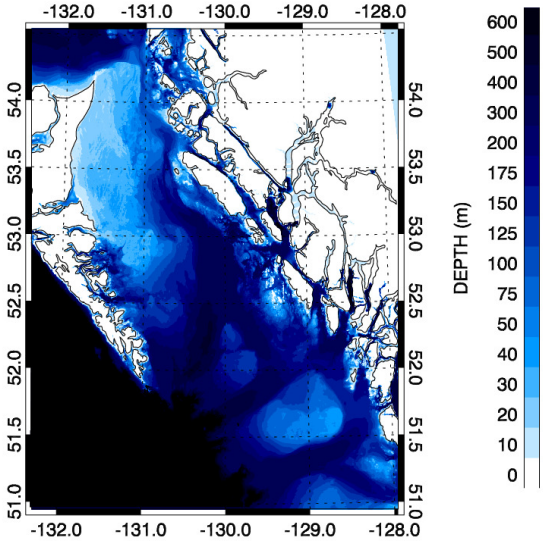

Figure 4: Contour map of bathymetry in Queen Charlotte Basin.

4.3.2. Ocean sound speed profiles

Representative sound speed profiles for the Queen Charlotte Basin were derived from a set of over 3000 CTD (Conductivity-Temperature-Depth) casts from Fisheries and Oceans Canada research cruises during 1982–1995. The extensive collection of temperature and salinity data was obtained from a CD-ROM report on the oceanography of the Queen Charlotte region compiled by W. Crawford of the Institute of Ocean Sciences [2001]. Temperature and salinity profiles were sorted by time of year and converted to sound speed using Coppens' equation for the speed of sound in seawater [1981].

Temperature and salinity profiles in the ocean typically exhibit seasonal patterns so, in order to derive representative sound speed profiles for the QCB, it was necessary to select a time of year when seismic exploration is most likely to be conducted. From a geophysicist's standpoint, the most favourable period for conducting a seismic survey in the QCB is during the summer and early autumn when the weather is mildest (K. Rohr, Rohr Consulting, personal communications, Jan. 2005). Thus, temperature and salinity profiles from July through September were analyzed to determine representative sound speed profiles.

Even when seasonal subsets of the sound speed profiles were extracted, there remained a large volume of data to analyze. Thus, a statistical technique known as *principal component analysis* (PCA) was used to derive representative profile shapes. The theory behind principal component analysis, also called empirical orthogonal function analysis, has been described in detail by other authors [Davis, 1976] and will not be discussed here. In summary, PCA is used to derive modes of variability, called eigenvectors, from a set of correlated data. The principal components are "derived variables", which express the observed data in terms of these eigenvectors. PCA is powerful because often only a few principal components are necessary to describe the observed variability in a dataset. Thus, the effect of PCA is to reduce the dimensionality of a dataset from many real variables (*e.g.*, sound speed versus depth) to only a few derived variables (the principal components).

All of the sound speed profiles were resampled at identical depth intervals before PCA was applied. Regular subdivisions of standard oceanographic depths up to 500 metres were used, yielding 26 sound speed sample points versus depth for each profile. Next, a 26×26 covariance matrix was constructed from the resampled sound speed profiles and the eigenvectors were found by performing eigenvalue decomposition on this matrix. Finally, the principle components were determined by projecting the data onto the eigenvectors. Upon performing this analysis, it was found that the first principal component accounted for 89% percent of the variability in the sound speed profiles. Figure 5 shows the distributions of values of the first principal component, and the shape of the corresponding eigenvector.

Two representative profile shapes, shown in Figure 6, were derived based on the 95% range of observed values of the first principal component. These two profiles represent "down-refracting" and "surface-duct" sound transmission scenarios and have been denoted profile A and profile B respectively. Under profile A conditions, the sound speed maximum near the surface will refract acoustic energy towards the sea bottom. Conversely, under profile B conditions, the sound speed minimum near the surface (called a surface duct) will trap acoustic energy and transmit it to longer ranges.

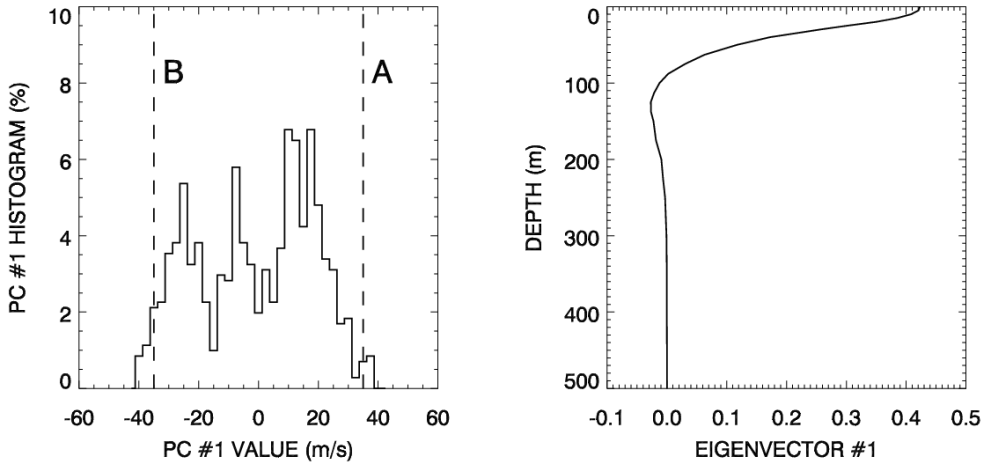

Figure 5: (Left) Histogram showing the distribution of values of the first principal component. (Right) Plot showing the shapes of the corresponding eigenvectors — note that the eigenvector units are dimensionless. The dashed vertical lines in the left plot, which bracket approximately 95% of the observed data, indicate the principal component values that were used to derive profile shapes A and B respectively (see Figure 6).

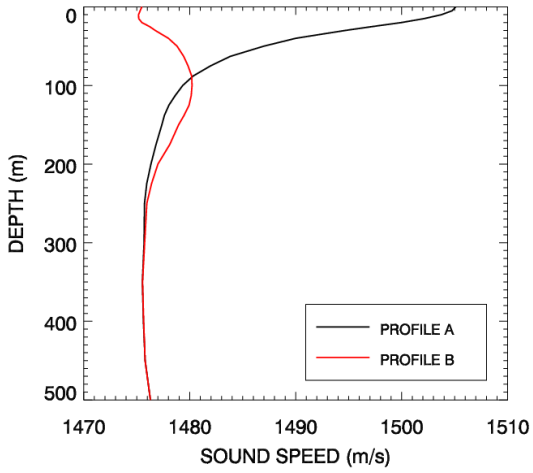

Figure 6: Plot of the two sound speed profiles, designated A and B, employed for the transmission loss modelling in this study.

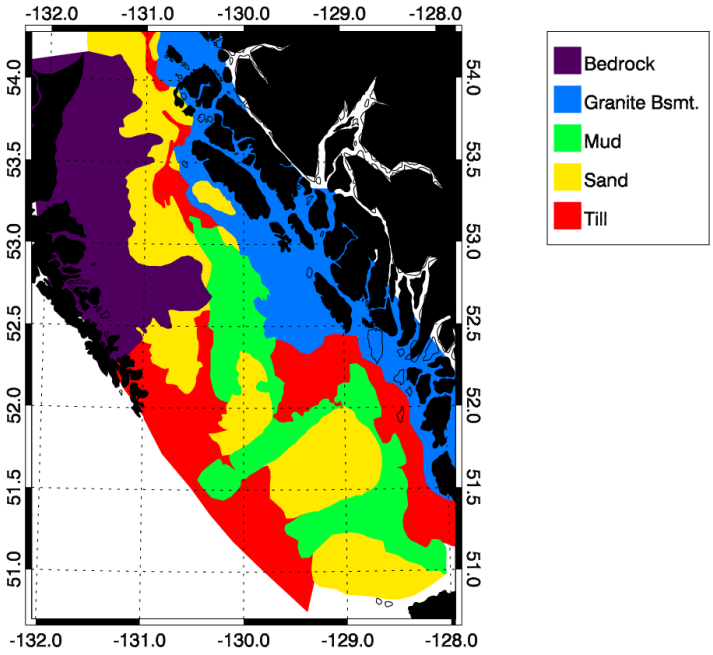

Figure 7: Map of geoacoustic provinces that were defined for the Queen Charlotte Basin, based on surficial geology maps published by the Geological Survey of Canada.

4.3.3. Geoacoustic database

Geoacoustic profiles were derived from a geoacoustic database for the Queen Charlotte Basin that was created, based on extensive geological surveying and mapping work that has been conducted in this region. Several studies of the surficial geology of the QCB have been published; *e.g.*, Barrie & Bornhold [1989], Bornhold & Barrie [1991] and Barrie *et al.* [1991]. The QCB covers a vast area and its surficial geology is quite complicated; however some general statements about the geology of the seafloor are possible:

1. The bedrock to the QCB predominantly consists of lithified Tertiary sediments.
2. Glacial till overlies the basement in deeper water.
3. Unconsolidated recent sands and gravels overlie the basement in the shallow waters to the north of the basin, and on the banks to the south.
4. In the troughs, unconsolidated recent silt and mud have been deposited on the glacial till.

The surface sediment coverage in the QCB is non-uniform in many places, and the thickness is variable. Furthermore, no maps of the sediment thickness exist and there are no direct measurements available of the acoustic properties of the surface materials. Thus, in order to generate a comprehensive geoacoustic database for the basin, it was necessary to generalize the seabed into a handful of provinces, each representing a typical bottom layering profile. Five kinds of provinces were defined for Dixon Entrace, Hecate Strait and Queen Charlotte Sound, each associated with a different bottom type: “Sand”,

"Mud", "Till", "Bedrock" and "Granite Basement". The spatial coverage of these geoacoustic provinces, shown in Figure 7, was based on surficial geology maps of the Queen Charlotte Basin published by the Geological Survey of Canada [Luternauer *et al.*, 1990].

Each geoacoustic province was associated with a single stratified seabed model, comprised of horizontal layers of sediments and rock. Since the geoacoustic parameters of the various layers were not directly measured, they had to be estimated based on sediment type. There have been extensive measurements of the geoacoustic parameters of common sediment types, which are summarized in a comprehensive review article by Hamilton [1980]; this article remains the definitive reference for geoacoustic modelling, to this day. Based on the measured bottom parameters given in Hamilton's paper, geoacoustic profiles were postulated for the five province types. Appendix C lists the geoacoustic profiles that were used in each province, with the corresponding values for the five main geoacoustic parameters: compressional wave speed, c_p, shear wave speed, c_s, density, ρ, compressional attenuation, α_p, and shear attenuation, α_s.

4.4. Model execution

For each source location, setting up the transmission loss model involved extracting all of the necessary information from the physical environment databases and preparing it for input into RAM. To do this, a separate setup program was written in the IDL programming language that performed the following four tasks:

1. Modelling radials were extended from the source position to the limits of the basin, over 360º of arc at 2.5º spacing.
2. Bathymetry and geoacoustic data were extracted from the physical environment databases at 50 m intervals along the modelling radials.
3. A single sound speed profile, either A or B, was selected for the whole basin.
4. The physical environment data for all the radials were written to a "job" file, for batch execution by RAM.

Note that all of the physical environment databases and modelling radials were defined on a UTM (Zone 9) x/y coordinate grid. For each job file, the transmission loss model RAM was executed in batch fashion at 22 frequencies for all 144 radials. The transmission loss grids computed by RAM were concatenated together into a single output file for each job. Yet another program, written in Fortran, combined the transmission loss data output by RAM with the source levels computed by the source model to generate grids of received sound level values.

5. Selection of source locations

For the transmission loss modelling, source locations were positioned along two simulated survey track lines, one running along the axis of the basin in the NNW–SSE direction and the other running across the basin in the NE–SW direction; these two track lines were designated "NS" and "EW" respectively. These particular track lines were selected based on discussions with Dr. Kristin Rohr on the results from the most recent geophysical study of the hydrocarbon potential in the Queen Charlotte Basin (K. Rohr,

personal communications, Jan. 2005). The two track lines traverse zones of the basin that have a high potential for oil and gas deposits [Whiticar *et al.*, p. 102] and intersect at the location of the Sockeye B10 exploratory well[2]. Table 3 lists the coordinates and labels of the source locations, along with the array heading and water depth at each position. Each source position has been designated with a unique label, except for the intersection of the track lines, which has two labels: NSL03 and EWL03. This is to distinguish between the two cases where the airgun array is aligned along the two different track lines. Figure 8 shows a map of the survey track lines, with the source positions superimposed.

Table 3: List of geographic coordinates, array heading and water depth at each source location. Locations EWL03 and NSL03 are at the same position but have different array headings. Note that array headings are given in degrees counter clockwise from UTM easting (*i.e.*, in the Cartesian sense) and are not North-referenced.

Location	Lon. (deg)	Lat. (deg)	θ_0 (deg)	Depth (m)
EWL01	-130.579	53.073	42.8	115.9
EWL02	-130.796	52.946	42.8	48.8
EWL03	-131.012	52.819	42.8	32.9
NSL01	-131.339	53.315	108.5	27.3
NSL02	-131.178	53.067	108.5	37.8
NSL03	-131.012	52.819	108.5	32.9
NSL04	-130.903	52.615	108.5	96.0
NSL05	-130.794	52.411	108.5	108.4
NSL06	-130.645	52.174	108.5	192.0

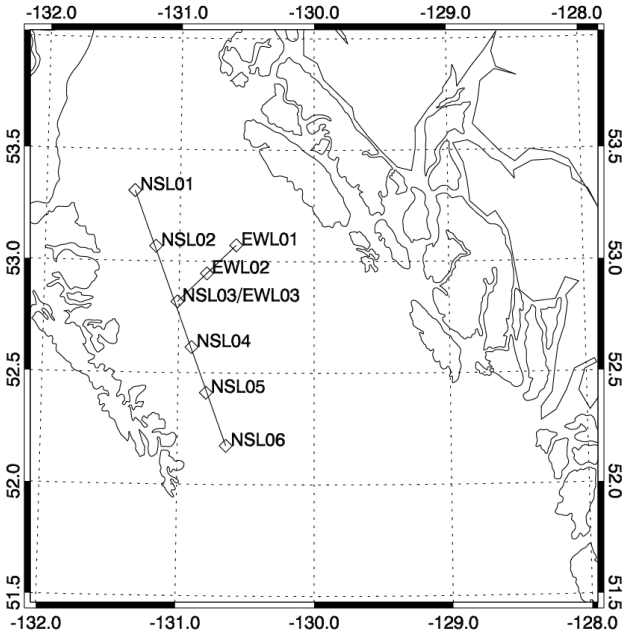

Figure 8: Map of survey track lines, along with labelled source locations, used for the current study.

[2] Cores from the Sockeye B10 well, drilled by Shell Canada Ltd. in 1968, showed oil stains, indicating the likely presence of hydrocarbon deposits at this location.

6. Results

RAM was executed at eight unique source locations, for both the A and B sound speed profile shapes, yielding a total of 16 of transmission loss grids. The transmission loss grids were then combined with the directional source levels for the airgun array, using equation 1, to yield 1/3-octave band pressure levels as a function of receiver position:

$$L_{bf_c}(r, z, \theta, f_c) = SL(f_c, \theta - \theta_0) - TL(r, z, f_c, \theta) \qquad (10)$$

where (r, z, θ) are the coordinates at the receiver position, f_c is the band frequency and θ_0 is the azimuthal heading of the airgun array. Finally, the 1/3-octave band pressure levels were summed together, using equation 6, to yield the total received level, *RL*, as a function of receiver position:

$$RL(r, z, \theta) = \sum_{f_c} 10^{L_{bf_c}(r, z, f_c, \theta)/10} \qquad (11)$$

Figure 9 shows an example of the received level cross-sections, in range and depth, for the EWL03 source location. Both cross sections are for the same SW-oriented modelling azimuth (315° clockwise from UTME) and demonstrate the difference in the range and depth distribution of the acoustic energy for the two different profile shapes. In the profile A cross-section, the acoustic energy has clearly been refracted toward the seabed, and the maximum sound levels are encountered near the sea-bottom. Conversely, in the profile B cross-section, the acoustic energy has been trapped in the surface duct and the maximum sound levels are encountered near the sea-surface.

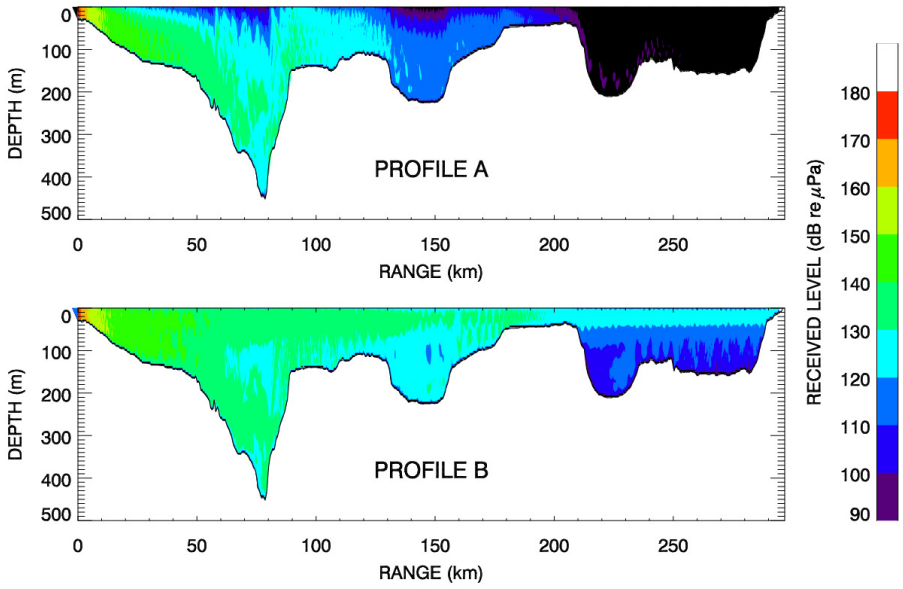

Figure 9: Broadband received level cross-sections, in range and depth, for the EWL03 source location. Received level plots are for the θ = 315° modelling azimuth, for profile A (top) and for profile B (bottom).

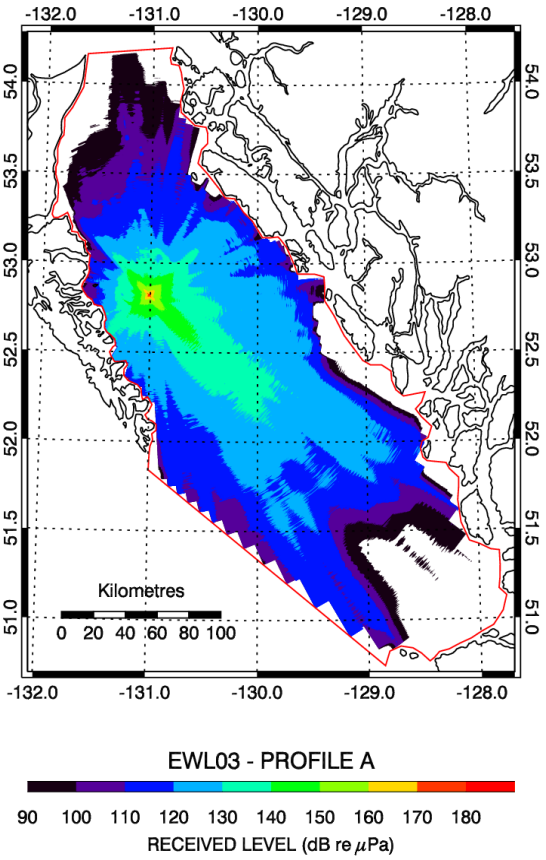

Figure 10: Geographic contour plot of received sound level for the EWL03 source position, under sound speed profile A conditions.

The fan of radials from each source position was combined to generate contours of the received level, such as the example shown in Figure 10. Geographic contour maps of the received sound levels, for all 18 modelling scenarios, are provided in Appendix D. The effect of the array directionality on the shape of the received level contours is immediately apparent — lobes of increased sound intensity clearly emanate from the broadsides of the array (*i.e.*, in the in NW–SE direction in Figure 10). As well, one can see that received levels are much lower in the shallow waters of Dogfish banks, to the north of the basin. This is because low frequency sounds, which contain most of the acoustic energy from the airgun array, propagate as highly attenuated leaky modes in shallow water and are rapidly absorbed into the bottom. Note that, in order to represent the data in two-dimensions, the received level at each geographic position (r, θ) was taken to be the maximum received level at any depth, z. This approach is conservative, since it makes no assumption as to what depth a marine mammal or fish may be found in the water column.

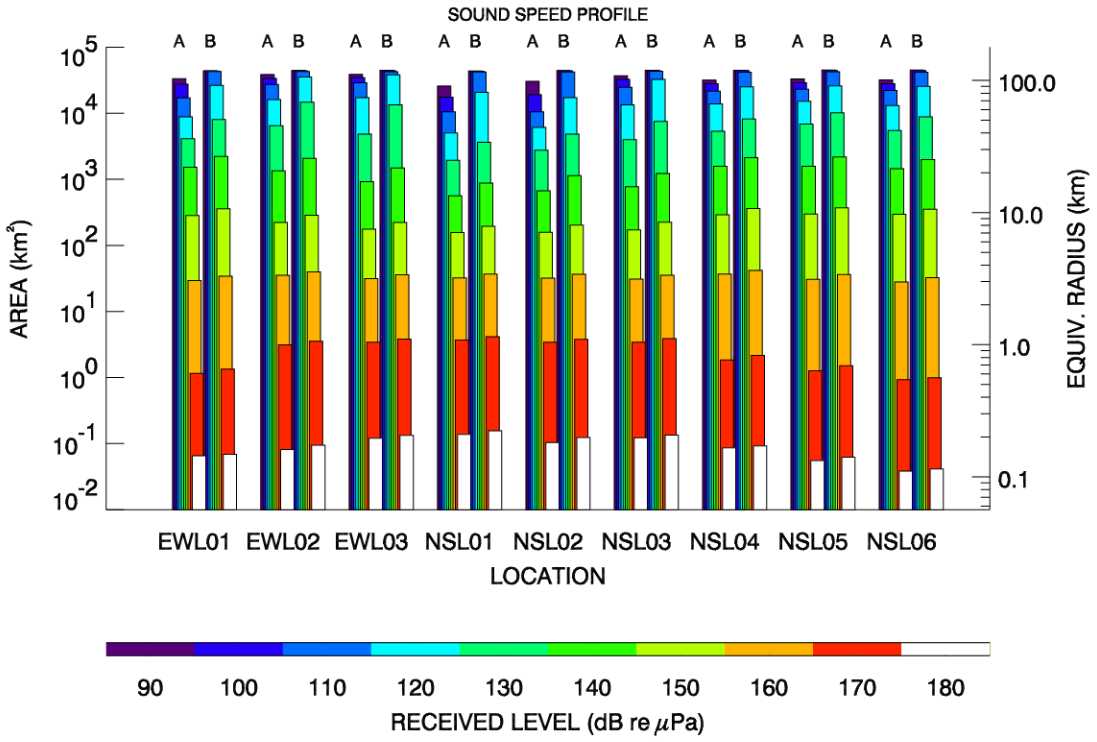

Figure 11: Bar plots of total area ensonified between 180 dB and 90 dB for all modelling scenarios considered in the current study. Two bars are presented for each source location, corresponding to the two sound speed profile shapes A and B (see Figure 6). The total area of each sound level contour, in square kilometres is indicated on the left hand axis; the right-hand axis shows the "equivalent radius", in kilometres, of a circle with the same total area. Note that the received level metric is SEL in dB re µPa·√s (see discussion in § 3.4.1).

A more succinct summary of the modelling results may be found in Figure 11, which presents a bar graph showing the total ensonified area, from 180 dB to 90 dB in 10 dB increments, for all 18 modelling scenarios. Two bars are shown for each source location, one each for the down-refracting and surface-duct sound speed profile shapes (A and B, respectively). The length of each bar is proportional to the area enclosed by the corresponding received level isopleth. Note that the total area of the basin imposes an upper limit on the length of the bars in Figure 11. Areas are given in units of square kilometres, as shown on the left hand axis of the plot. Since areas can be difficult to visualize, the radius of a circle with the same area (*i.e.*, $r = \sqrt{A / \pi}$) is shown on the right hand axis in units of kilometres. This "equivalent radius" can be also thought of as a mean contour radius, averaged over azimuth angle.

Examining Figure 11, one can see that the area of the 180 dB and 170 dB received level isopleths is greater when the source is located at shallower water depths (*c.f.* Table 3). This is because, in an ocean waveguide, the transition range between stronger spherical spreading loss ($TL \sim 20 \log r$) and weaker cylindrical spreading loss ($TL \sim 10 \log r$) is proportional to the water depth. In other words, in shallower water depths, critical angle reflection of sound from the seabed occurs at a shorter distance from the source and so more acoustic energy is concentrated in the water column. Thus, at ranges less than a

few kilometres, received levels from the array are more intense in shallower water. However, one can see that this trend is reversed beyond the 160 dB isopleth, at ranges greater than a few kilometres. The reason for this is that in shallow water the sound speed profile directs the seismic survey noise downward to the seabed and so there is more significant interaction with the seabed. Since the seabed (which is elastic and sloping) is not a perfect reflector, there is an increasing attenuation of the acoustic intensity with range. By comparison, sound trapped in a surface duct is free from bottom interactions and is carried to far greater distances. This effect is quite pronounced at ranges approaching 100 km, where the difference in received level is often 20 dB or more between profile A and profile B scenarios.

Figure 12 shows the frequency evolution of the seismic pulse with range along the range/depth modelling cross-section of Figure 9. The depth of the receiver for both plots is 25 metres. One can see from Figure 12 that peak received levels along this azimuth occur at frequencies between 100 Hz and 200 Hz, and that low frequencies, below 50 Hz, are rapidly attenuated with range. As in Figure 9, the effect of the sound speed profile on the band pressure levels is most evident at long ranges.

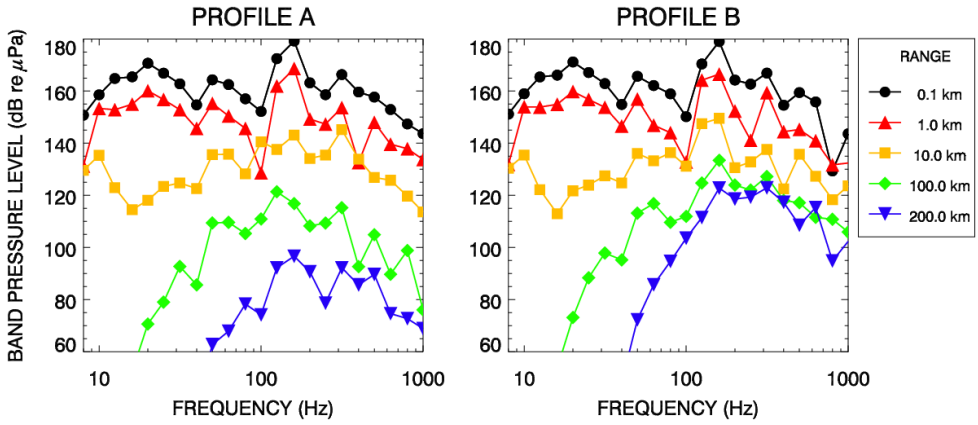

Figure 12: Frequency evolution of the seismic pulse versus range along the SE oriented track line of Figure 9. Two plots are shown, one for profile A (left) and one for profile B (right). The receiver depth is 25 metres.

Table 4: Table illustrating 90% RMS SPL values and corresponding SEL values for NMFS threshold noise levels given in this report, assuming a 100 msec pulse length. Note that modelling results presented in this report are reported as SEL values for a single airgun pulse (equivalent to 1-second SPL). See text and also Section 3.4.1 for discussion.

NMFS Threshold Level	90% RMS SPL	Equivalent SEL
Cetaceans (whales and porpoises)	180 dB re µPa	170 dB re $\mu Pa^2 \cdot s$
Pinnipeds (seals and sea-lions)	190 dB re µPa	180 dB re $\mu Pa^2 \cdot s$

7. Discussion

7.1. Seismic noise and marine animals

The US National Marine Fisheries Service (NMFS) has established threshold noise levels above which they estimate that marine mammals may be subject to temporary hearing threshold shift or possible auditory damage [60 Fed. Reg. 53753–60]. NMFS recommends that cetaceans (*i.e.*, whales and porpoises) not be exposed to sound pressure levels in excess of 180 dB and that pinnipeds (*i.e.*, seals and sea-lions) not be exposed to sound pressure levels in excess of 190 dB. These guidelines are based on estimates of marine mammal hearing damage thresholds extrapolated from known Damage Risk Criteria for humans [Richardson *et al.*, 1995, §10.6].

The NMFS thresholds are cast in terms of sound pressure levels over the 90% pulse duration (see §3.4.1), which are not equivalent to the SEL values given in this study. However, one can use equation 5 to convert these thresholds to SEL, if an appropriate value for the duration of the seismic pulse is assumed. A heuristic value of ~100 msec was selected for the pulse duration, T_{90}, based on measurements at ranges less than a few kilometres. This value must be considered approximate — for example, the investigator C.R. Greene measured pulse durations between 500 msec and 100 msec at ranges between 500 m and 2 km, for pulses from an airgun array operating in ~400m water depth off Southern California [Greene, 1998, Fig. 5]. Though Greene measured shorter pulse durations at shorter ranges, he also states that, "for pulses greater than about 0.1 s…the SPL measure is accepted as the important pulse measure to relate to influences on animal behaviour and even injury to animals" [Greene, 1998, p. 9]. Therefore, a 100 msec pulse duration is a conservative choice, since the 90% RMS SPL may not be as applicable for shorter time windows.

For a pulse duration of 100 msec, equation 5 shows that the conversion factor between 90% RMS SPL and SEL is approximately –10 dB. Thus the SEL thresholds corresponding to the NMFS guidelines are roughly 180 dB for pinnipeds and 170 dB for cetaceans, as illustrated in 4. Table 5 shows the equivalent radii, from Figure 11, at which these sound thresholds are encountered for each source location. Ranges to the 180 dB SEL isopleth vary from 110 metres at the deepest location (NSL06) to 223 metres at the shallowest location (NSL01); ranges to the 170 dB SEL isopleth vary from 544 metres at the deepest location (NSL06) to 1147 metres at the shallowest location (NSL01). These results are consistent with experimental observations, made during the calibration of the R/V Maurice Ewing's 20-gun research array, showing that received levels from an airgun array are greater in shallow water where "reverberations play a significant role in received levels" [Tolstoy *et al.*, 2004].

Table 5: Equivalent radii for 180 dB and 170 dB SEL isopleths, from Figure 11, for each source location.

Source Location	180 dB Eqiv. Rad. (m)		170 dB Eqiv. Rad. (m)	
	Profile A	*Profile B*	*Profile A*	*Profile B*
EWL01	144	147	607	655
EWL02	161	174	997	1062
EWL03	196	206	1041	1100
NSL01	209	223	1085	1147
NSL02	182	198	1043	1097
NSL03	197	207	1043	1109
NSL04	166	171	765	830
NSL05	133	140	634	693
NSL06	110	115	544	561

It is important to be aware that the NMFS 190 dB and 180 dB levels are somewhat speculative, since they are not based on actual measurements on marine mammals. In addition, they do not take into account the variation in hearing ranges and hearing thresholds (*i.e.*, audiograms) between different species of marine mammals. In fact, the current NMFS noise level regulations with regards to seismic noise are currently under review and will be revised in the near future based on a more up-to-date scientific understanding of the effect of noise on marine mammals. Furthermore, it is expected that the new NFMS criteria will be based on a sound exposure metric, rather than the current RMS sound pressure metric [W.J. Richardson, LGL Ltd., personal communications, Mar. 2005].

At lower received levels, seismic noise may elicit behavioural reactions in marine mammals; documented disturbance effects include startle response, avoidance of the seismic survey source, cessation of feeding and changes in diving and breathing patterns [Gordon *et al.*, 2004, Tab. 2]. Unfortunately, behavioural effects are not predictable and vary significantly between animals, even among individuals of the same species. The report of the High Energy Seismic Survey Team, prepared for the California State Lands Commission and the US Minerals Management Service, had the following to say:

> The expert panel convened at the HESS workshop … concluded that behavioral responses by marine mammals to seismic sounds would most likely occur at received levels above 140 dB re 1 µPa (rms). As discussed in Richardson et al. (1995), however, the limited evidence available indicates that there are differences in responsiveness to seismic sounds among marine mammal groups, with baleen whales, and perhaps sperm whales, being the most sensitive and eared seals the least. [*HESS, 1997, p. 29*].

At ranges of ten kilometres or more, where received levels of 140 dB are expected to be encountered, the –10 dB conversion factor between SEL and RMS SPL is probably too conservative. This is because spreading of the seismic pulse, due to dispersion and scattering, will likely extend the effective pulse length at these ranges. From Figure 11, one can see that the modelled 140 dB received level isopleths extend over areas ranging from 500 km^2 (~12.6 km equivalent radius) to over 2000 km^2 (~23.2 km equivalent radius). However, identifying whether behavioural disturbances due to seismic noise at these ranges could possibly result in biologically significant consequences for marine mammals is beyond the scope of this study.

As yet, there are no equivalent guidelines for exposure of fish to seismic airgun noise as there are for marine mammals. Controlled exposure tests of caged fish to airgun noise at close proximity have demonstrated that fish ears are susceptible to damage from high intensity impulsive noise [Popper *et al*., 2004, p. 37]. Indeed, the hearing of many fish is most acute at low frequencies, down to 100 Hz, where airgun noise is concentrated [NRC 2003, p. 87]. Studies in the wild have demonstrated that catch rates of fish temporarily decline in the vicinity of a seismic survey, suggesting that fish may avoid airgun noise [Popper *et al*., 2004, p. 38]. However, much is still unknown about the overall effect of seismic survey noise on fish.

Another kind of marine organism, of special concern in the Queen Charlotte Basin, is the siliceous (glass) sponge. The large sponge reefs, which have recently been discovered in the benthic waters of Hecate Strait and Queen Charlotte Sound, are thought to be unique to this region. The silica skeletons of these sponges are not likely to be damaged by exposure to airgun pulses, since airguns do not produce the shock front that is generated by an explosive charge. Smothering caused by increased sediment concentrations in bottom waters is thought to pose a risk to siliceous sponges [Whitney *et al.*, in publ.] but the operation of airguns at the surface is unlikely to stir up sediments at the depths > 160 m where the sponges are located.

7.2. Ambient noise levels in QCB

Ultimately, whether or not seismic survey noise will be detectable by marine animals depends on the loudness of that noise relative to the ambient background noise (*i.e.*, due to both natural and anthropogenic sources). If the 1/3-octave band loudness of a seismic pulse falls below the corresponding 1/3-octave band ambient noise level then it will likely not be audible by a marine animal [Richardson *et al*., 1995, p. 326]. According to the passive sonar equation, which applies equally well for marine mammals and fish as it does to sonar systems, the signal excess at the receiver, *SE*, for an underwater signal is [Urick p. 21]:

$$SE = RL - NL - DT \qquad (12)$$

This equation simply states that if the received level of a sound, *RL*, minus the noise level, *NL*, is less than the detection threshold *DT*, then it is not audible (i.e., detectable). For marine mammals detection thresholds are limited to about 0 dB, especially at lower frequencies [Richardson *et al*. 1995, p. 327]. The region where $SE > 0$ defines the zone of audibility, outside of which anthropogenic noise from the seismic survey cannot be heard. However, in order to determine this zone, prior knowledge of the ambient noise level is required. Unfortunately, to date there have been no dedicated measurements of baseline ambient noise levels in the Queen Charlotte Basin.

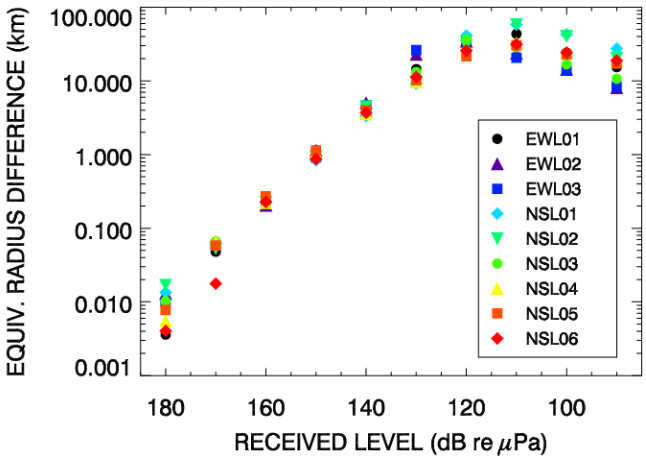

Figure 13: Difference in equivalent isopleth radius, between profile A and profile B, for each modelling location considered in the current study (*c.f.*, Figure 11). Note that the levelling off of the differences below 120 dB is an artefact due to the received level contours intersecting the boundary of the modelling region.

7.3. Sources of uncertainty in acoustic model predictions

Though acoustic models are capable of reproducing sound transmission observed in real ocean environments, the accuracy of a propagation model is often limited by knowledge of the environmental parameters. Thus, uncertainty is introduced into acoustic propagation modelling in two ways:

1. When the environmental parameters are variable in time — *e.g.*, the sound speed profile or sea surface roughness.
2. When the environmental parameters are poorly constrained — *e.g.*, the geoacoustic parameters.

For time varying parameters, if the limits of the variation are known, it is possible to estimate the resulting uncertainty in the received level. In the current study, the uncertainty due to the variation in sound speed profile was bracketed by using the two limiting profile shapes, A and B, in the propagation modelling. Figure 13 shows the difference in equivalent isopleth radius (*c.f.*, Figure 11) between profile A and profile B, for each modelling location. It is apparent from this figure that the influence of the sound speed profile on received level, due to ducted propagation, increases dramatically with distance from the source.

The effect of sea-surface roughness, due to wind and waves, on the acoustic propagation was not considered in the present study, as RAM does not currently have the ability to model this phenomenon. However, the effect of a rough sea surface is to scatter incident sound. Thus, surface scattering would have the greatest affect on ducted propagation (*i.e.*, profile B conditions) by releasing trapped acoustic energy from the surface duct. Therefore, rough seas are expected to reduce received sound levels in the presence of profile B conditions, though the true magnitude of this effect has not been modelled.

The physical environment data of greatest uncertainty in the QCB are the geoacoustic parameters of the seabed. Though geoacoustic profiles were estimated for the current study, based on knowledge of the geology of QCB, it would be far better to have actual measurements of these data. Geoacoustic parameters may be measured directly, from sediment core data, or remotely using shallow seismic profiling or geophysical inversion. In addition, the accuracy of a of a geoacoustic model in predicting sound propagation may be evaluated by comparing predicted transmission loss to *in situ* measurements of acoustic propagation. By using geoacoustic data obtained from a field study in QCB, it would be possible to refine the transmission loss predictions of this study and remove a significant source of uncertainty in the model predictions.

8. Conclusions

The current study was undertaken to model the generation and propagation of underwater noise from a seismic airgun survey in the Queen Charlotte Basin. This study was conducted to help address the issue of the potential effects seismic surveying would have on marine mammals and fish in this region. Noise level predictions presented in this report were based on an integrated modelling approach that incorporated an airgun array source model, a broadband transmission loss model and databases describing the physical environment. Maps of received noise levels were computed for nine different source scenarios at positions along two simulated survey tracks. The modelled survey tracks traversed a region of the basin believed to have a high potential for future oil and gas exploration.

In addition to the received levels presented in this report, this study has also developed a flexible methodology for predicting sound levels generated by any future seismic survey in QCB. Considerable work has gone into compiling bathymetric, oceanographic and geoacoustic databases for the QCB, based on the most up-to-date physical data available. These phyical databases have been integrated with an N×2-D parabolic-equation acoustic propagation model, so that transmission loss can be modelled in three dimensions at any location in QCB. Furthermore, the transmission loss computed by the acoustic model may be combined with source levels for an arbitrary seismic source, using the airgun array source model discussed in this report. Thus, the methodology developed in this study will facilitate future seismic survey noise levels predictions, since it is in no way limited to the source geometry and survey locations considered in this report.

Key results of the modelling study may be summarized as follows:

- Received noise levels in the water were influenced by the source location, array orientation and the shape of the sound speed profile with respect to water depth.
- Received levels were lowest in those areas of the basin with shallow bathymetry (*e.g.*, Dogfish Banks) due to scattering and absorption of sound at the seabed.
- In contrast, surface-duct propagation conditions in deeper water resulted in the highest received noise levels at long ranges.
- The effect of the sound speed profile on received levels increased significantly with range from the source, with differences greater than 20 dB observed beyond 100 km, between down-refacting and surface-duct propagation conditions.

- Mean ranges to the 170 dB SEL isopleth (approximately equivalent to NMFS 180 dB 90% RMS threshold level) varied from 0.54 km to 1.15 km. The isopleth area was found to be greater in shallower water than in deeper water.
- The highest levels from the airgun array were in the broadside direction, which is the direction of maximum energy transmission from the array.

9. Literature cited

ANSI S1.1 (1994) *American National Standard Acoustical Terminology*.

Barrie, J.V. and Bornhold, B.D. (1989) "Surficial geology of Hecate Strait, British Columbia contintental shelf". Can J. Earth Sci. v.26 pp.1241-1254.

Barrie, J.V., Bornhold, B.D., Conway, K.W. and Luternauer, J.L. (1991) "Surficial geology of the northwestern Canadian continental shelf." Continental Shelf Res., v.11 pp. 701-715.

Bornhold, B.D. and Barrie J.V. (1991) "Surficial sediments on the western Canadian continental shelf." Continental Shelf Res., v.11 pp. 685-699.

Collins, M.D. (1993) "A split-step Pade solution for the parabolic equation method," J. Acoust. Soc. Am. 93, 1736–1742.

Coppens, A.B. (1981) "Simple equations for the speed of sound in Neptunian waters." J. Acoust. Soc. Am. 69(3), 862-863.

Crawford, W.R. (2001) "Oceans of the Queen Charlotte Islands." Canadian Technical Report of Fisheries and Aquatic Sciences No. 2383.

Davis, R.E. (1976) "Predictability of sea surface temperature and sea level pressure anomalies over the North Pacific Ocean," J. Phys. Ocean. 6 (3) pp. 249-266.

Dragoset, W.H. (1984) "A comprehensive method for evaluating the design of airguns and airgun arrays." 16th Annual Proc. Offshore Tech. Conf. 3, 75-84.

Federal Register (1995) "Small Takes of Marine Mammals Incidental to Specified Activities; Offshore Seismic Activities in Southern California." vol. 60 pp. 53753–53760.

Gordon, J., Gillespie, D., Potter, J., Frantzis, A., Simmonds, M.P., Swift, R. and Thompson, D. (2004) "A review of the effects of seismic surveys on marine mammals." Marine Technology Society Journal, 37 (4) pp. 16–34.

Greene, C.R. Jr. (1998) "Sound Levels of an airgun array operating at platform Harmony on 17 March 1998." Appendix 7 in *High Energy Seismic Survey Review Process and Interim Operational Guidelines for Marine Surveys Offshore Southern California*. Feb. 1999 version.

Hamilton, E. (1980) "Geoacoustic modeling of the sea floor." J. Acoust. Soc. Am. 68, 1313-1340.

Hannigan, P.K., Dietrich, J.R., Lee, P.J., Osadetz, K.G. (2001) *Petroleum Resource Potential of Sedimentary Basins on the Pacific Margin of Canada*. Geological Survery of Canada Bulletin 564. Calgary: GSC.

HESS Team (1999) "Interim operational guidelines for high-energy seismic surveys off Southern California" Section 4 in *High Energy Seismic Survey Review Process and Interim Operational Guidelines for Marine Surveys Offshore Southern California*. Feb. 1999 version.

Landro, M., (1992) “Modelling of GI gun signatures.” Geophys. Prosp., 40 (7), 721-747.

Lurton, X. (2002) *An Introduction to Underwater Acoustics: Principles and Applications*. Springer, Chichester, U.K. 347 pp.

Luternauer, J.L. *et al.* (1990) “Surficial Geology of the Queen Charlotte Basin”, Geological Survey of Canada Open Files 2193, 2195, 2196 & 2197.

National Research Council (2003) *Ocean Noise and Marine Mammals*. National Academies Press, Washington D.C. 208 pp.

Popper, A.N., Fewtrell, J., Smith, M.E. and McCauley, R.D. (2004) “Anthropogenic sound: effects on the behaviour and physiology of fishes.” Mar. Tech. Soc. J., 37 (4) pp. 35–40.

Racca, R.G. and Scrimger, J.A. (1986) “Underwater Acoustic Source Characteristics of Air and Water Guns” Contractor report by JASCO Research Ltd., Victoria BC for DREP Contract No. 06SB 97708-5-7055.

Richardson, W.J., Greene, C.R. Jr., Malme C.J., and Thomson D.H. (1995) *Marine Mammals and Noise*. Academic Press, San Diego, CA. 576 pp.

Royal Society of Canada (2004) *The Royal Society of Canada Report of the Expert Panel on Science Issues Related to Oil and Gas Activities, Offshore British Columbia.* 155 pp.

Shulkin, M. and Marsh, H.W. (1962) “Sound Absorption in Sea Water.” J. Acoust. Soc. Am. 34 (6), 864-865.

Tolstoy, M., Diebold, J.B., Webb, S.C., Bohnenstiehl, D.R., Chapp, E., Holmes, R.C. and Rawson, M. (2004) “Broadband calibration of R/V Ewing seismic sources.” Geophys. Res. Lett., 31, L14310

Urick, R.J. (1967) *Principles of Underwater Sound for Engineers*. 1st ed. McGraw-Hill, New York. 317 pp.

Whiticar, M.J. *et al.* (2003) “Analysis of Petroleum Potential in Queen Charlotte Basin — Phase 1 Report Broad-Scale Basin Characterization.” Report sponsored by: Offshore Oil and Gas Team, Ministry of Energy and Mines, Government of British Columbia.

Whitney, F., Conway, K., Thomson R., Barrie V., Krautter M. and Mungov G. (2003) “Oceanographic Habitat of Sponge Reefs on the Western Canadian Continental Shelf.” Continental Shelf Res. *in publication*.

Ziolkowski, A. (1970) “A Method for Calculating the Output Pressure Waveform from an Air Gun.” Geophys. J. R. Astr. Soc. 21, 137–161.

Ziolkowski, A., *et al.* (1982) “The signature of an air gun array: Computation from near-field measurements including interactions.” Geophysics 47, 1413-1421.

Zhang, Y. and Tindle, C. (1995) “Improved equivalent fluid approximations for a low shear speed ocean bottom.” J. Acoust. Soc. Am. 98 (6), 3391-3396.

A. Far-field source level computation

The 1/3-octave band source levels for each modelling azimuth were computed from the horizontally propagating far-field signature of the array. The far-field signature, $s_{ff}(t)$ is the sum of the notional signatures of the individual guns, $s_i(t)$, time delayed according to their relative position and the propagation angle:

$$s_{ff}(t) = \sum_n s_i\left(t - \tau_i(\theta, \phi)\right)$$

where τ_i is its time-delay of the i^{th} gun in the angular direction (θ, ϕ). For horizontal sound propagation $\phi = 0$ and the time delay is only a function of the azimuthal angle, θ:

$$\tau_i = -\left(x_i \cos\theta + y_i \sin\theta\right)/c$$

where (x_i, y_i) is the position of gun i in the plane of the array and c is the speed of sound. A plan view diagram, illustrating the geometry of the far-field summation, is shown in Figure A-1. It is often more convenient to perform this calculation in the frequency domain by utilizing the Fourier transform shift theorem, which states that a time delay of τ corresponds to a phase delay of $2\pi f\tau$, so that:

$$S_{ff}(f, \theta) = \sum_n S_i(f) \exp\left(\frac{j2\pi f}{c}(x_i \cos\theta + y_i \sin\theta)\right)$$

where f is frequency and $S(f)$ denotes the Fourier transform of $s(t)$. The far-field signature is then filtered into 1/3-octave pass-bands to generate frequency dependent source levels:

$$SL(f_c, \theta) = 2\pi \int_{f_{lo}}^{f_{hi}} \left|S_{ff}(f, \theta)\right|^2 df$$

where $SL(f_c, \theta)$ is the source level in a 1/3-octave band with centre frequency f_c, in the azimuthal direction θ. Note that the limits of integration in this equation, f_{lo} and f_{hi}, are the lower and upper frequency bounds of the 1/3-octave band. Source levels, computed in this way, are suitable for combining with transmission loss output by a propagation model to compute received sound levels.

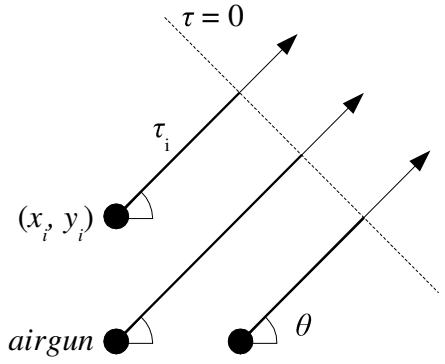

Figure A-1: Plan view diagram of the far-field summation geometry for an airgun array.

B. Airgun array directionality plots

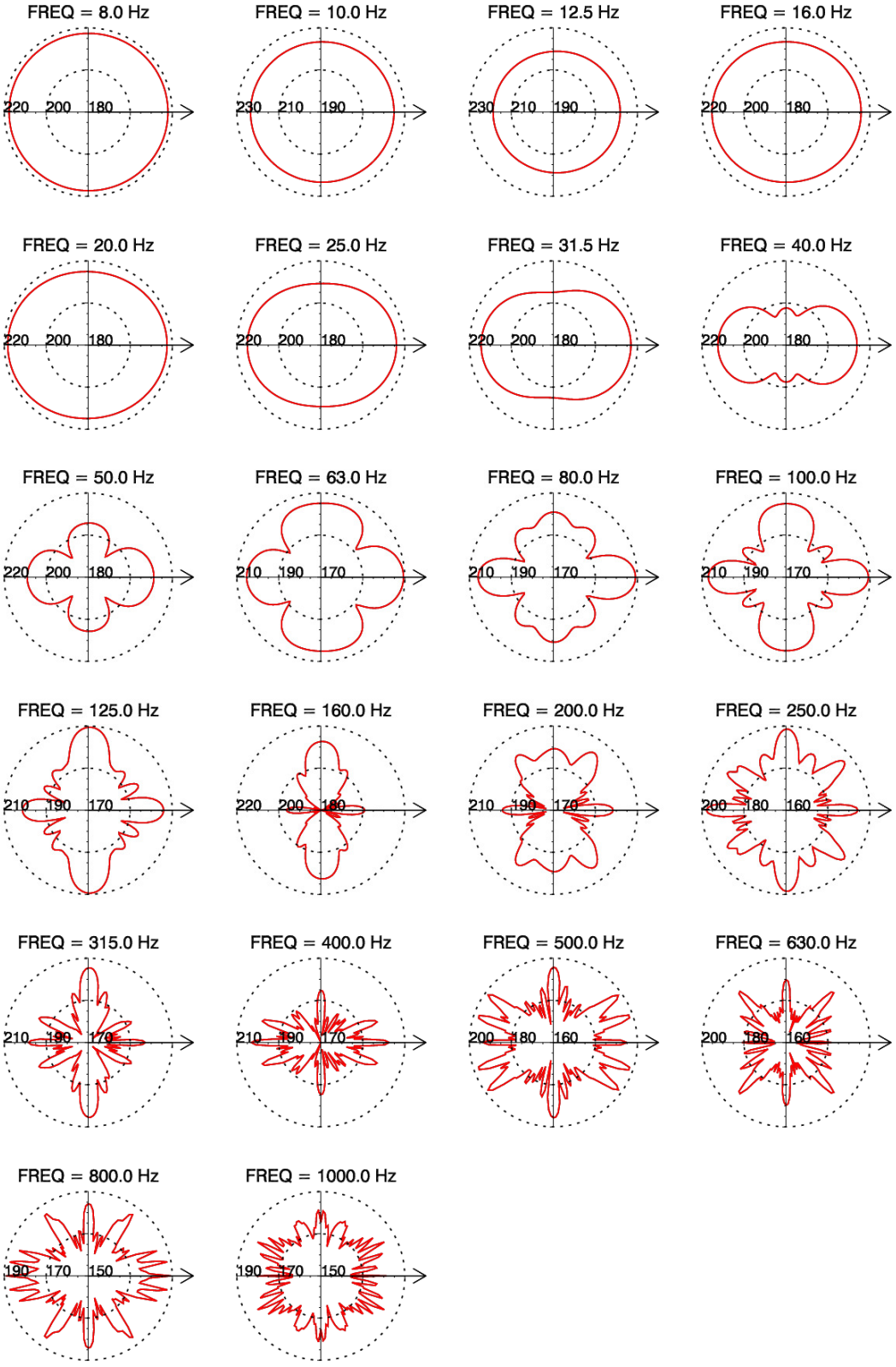

C. Geoacoustic profiles

PROVINCE: **Bedrock**

Material	z (m)	c_p (m/s)	ρ (g/cc)	α_p (dB/λ)	c_s (m/s)	α_s (dB/λ)
Sand	1	1715.1	1.941	0.429	52.8	0.697
	3	1743.6	1.941	0.436	62.4	0.824
	5	1757.1	1.941	0.439	71.0	0.938
Bedrock	5	2200.0	2.200	0.100	754.0	0.045
	100	2298.4	2.200	0.100	830.8	0.050
	200	2421.4	2.200	0.100	926.7	0.056

PROVINCE: **Granite Basement**

Material	z (m)	c_p (m/s)	ρ (g/cc)	α_p (dB/λ)	c_s (m/s)	α_s (dB/λ)
Till	0	1603.8	1.771	0.160	378.0	1.814
	3	1607.5	1.771	0.161	379.4	1.821
	5	1609.9	1.771	0.161	380.3	1.825
Granite	5	5500.0	2.600	0.050	2400.0	0.144
	500	6108.9	3.600	0.050	2665.7	0.160

PROVINCE: **Mud**

Material	z (m)	c_p (m/s)	ρ (g/cc)	α_p (dB/λ)	c_s (m/s)	α_s (dB/λ)
Mud	0	1526.7	1.596	0.198	172.7	2.989
	2	1529.2	1.596	0.199	182.3	3.154
	5	1532.9	1.596	0.199	196.6	3.402
	8	1536.6	1.596	0.200	211.0	3.650
	10	1539.0	1.596	0.200	220.5	3.815
Till	10	1662.1	1.771	0.166	401.3	1.926
	25	1680.6	1.771	0.168	409.3	1.965
Bedrock	25	2200.0	2.200	0.100	754.0	0.045
	500	2784.3	2.200	0.100	1209.7	0.073

PROVINCE: **Sand**

Material	z (m)	c_p (m/s)	ρ (g/cc)	α_p (dB/λ)	c_s (m/s)	α_s (dB/λ)
Sand	1	1700.3	1.941	0.425	52.4	0.692
	3	1728.6	1.941	0.432	55.9	0.738
	8	1754.2	1.941	0.439	69.0	0.910
	15	1770.8	1.941	0.443	82.5	1.089
	20	1778.5	1.941	0.445	90.1	1.190
Bedrock	20	2200.0	2.200	0.100	754.0	0.045
	100	2298.4	2.200	0.100	830.8	0.050

PROVINCE: **Till**

Material	z (m)	c_p (m/s)	ρ (g/cc)	α_p (dB/λ)	c_s (m/s)	α_s (dB/λ)
Till	0	1603.8	1.771	0.160	378.0	1.814
	5	1609.9	1.771	0.161	380.3	1.825
	10	1616.1	1.771	0.162	382.6	1.837
	12	1618.5	1.771	0.162	383.6	1.841
	15	1622.2	1.771	0.162	385.0	1.848
Bedrock	15	2200.0	2.200	0.100	754.0	0.045
	500	2796.6	2.200	0.100	1219.3	0.073

D. Sound level contour maps

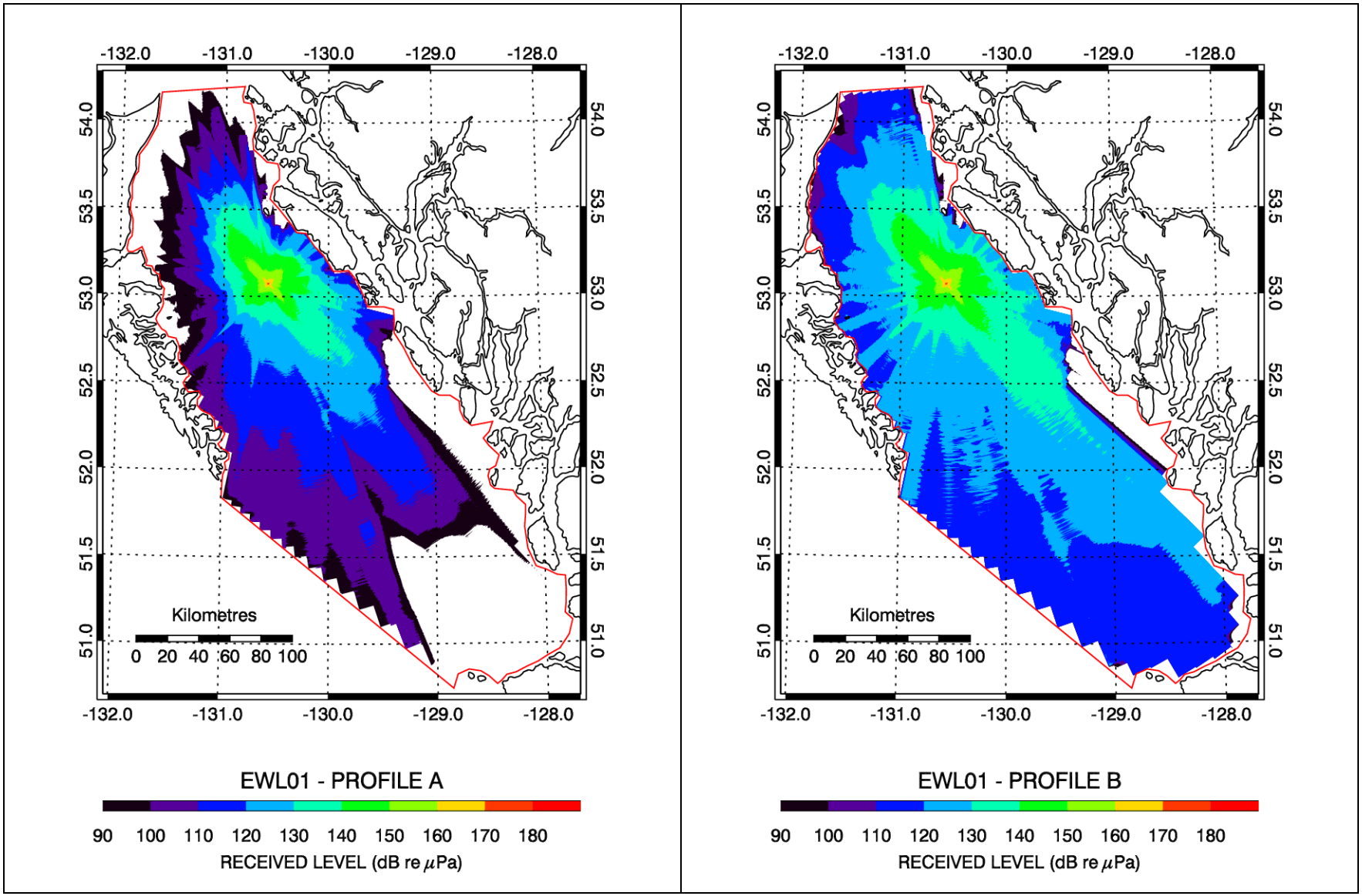
-132.0
-131.0
-130.0
-129.0
-128.0
54.0
53.5
53.0
52.5
52.0
51.5
51.0
Kilometres
0 20 40 60 80 100
EWL01 - PROFILE A
90 100 110 120 130 140 150 160 170 180
RECEIVED LEVEL (dB re μPa)
EWL01 - PROFILE B
90 100 110 120 130 140 150 160 170 180
RECEIVED LEVEL (dB re μPa)

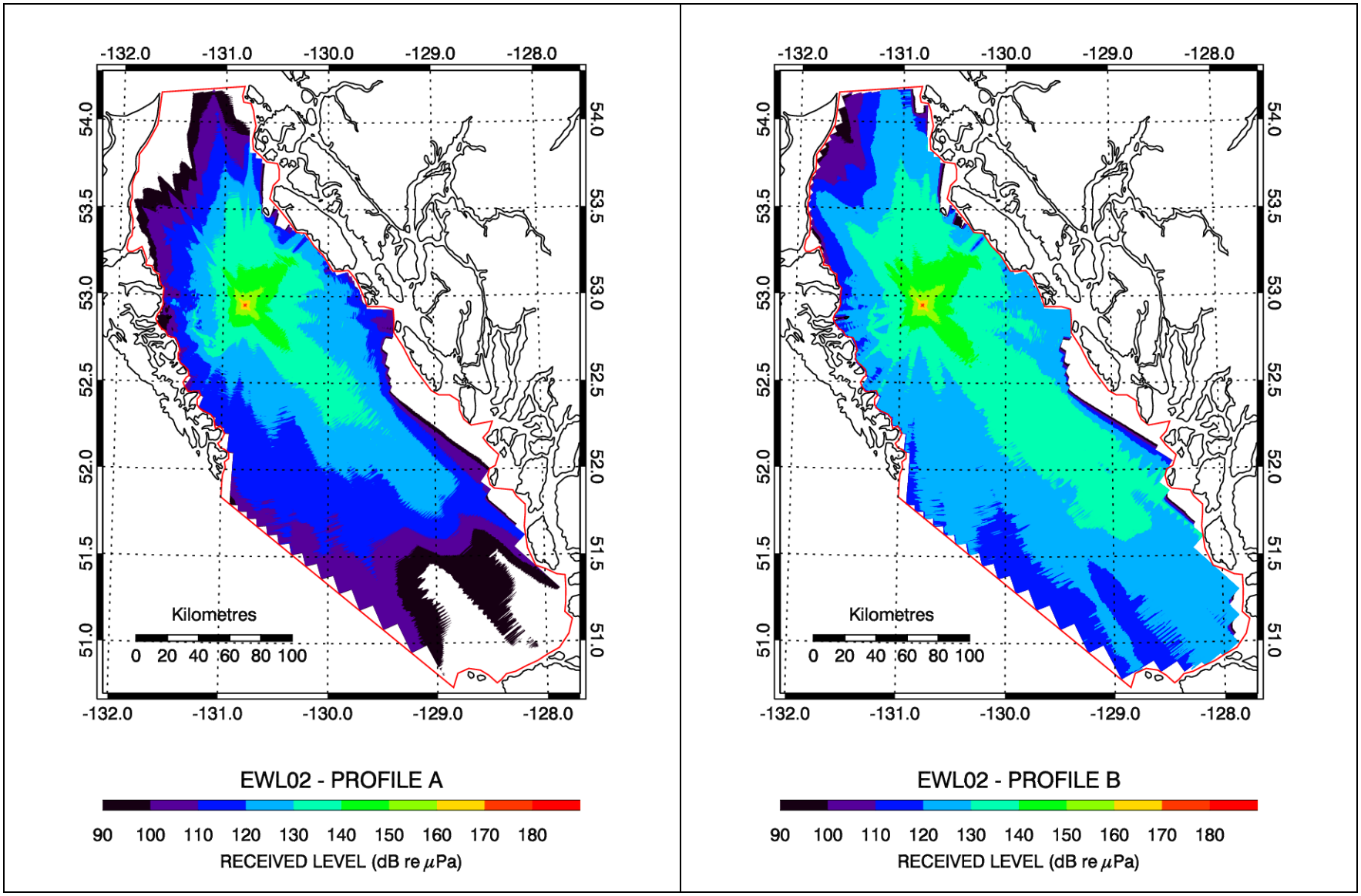
-132.0
-131.0
-130.0
-129.0
-128.0
54.0
53.5
53.0
52.5
52.0
51.5
51.0
Kilometres
0 20 40 60 80 100
EWL02 - PROFILE A
EWL02 - PROFILE B
90 100 110 120 130 140 150 160 170 180
RECEIVED LEVEL (dB re μPa)

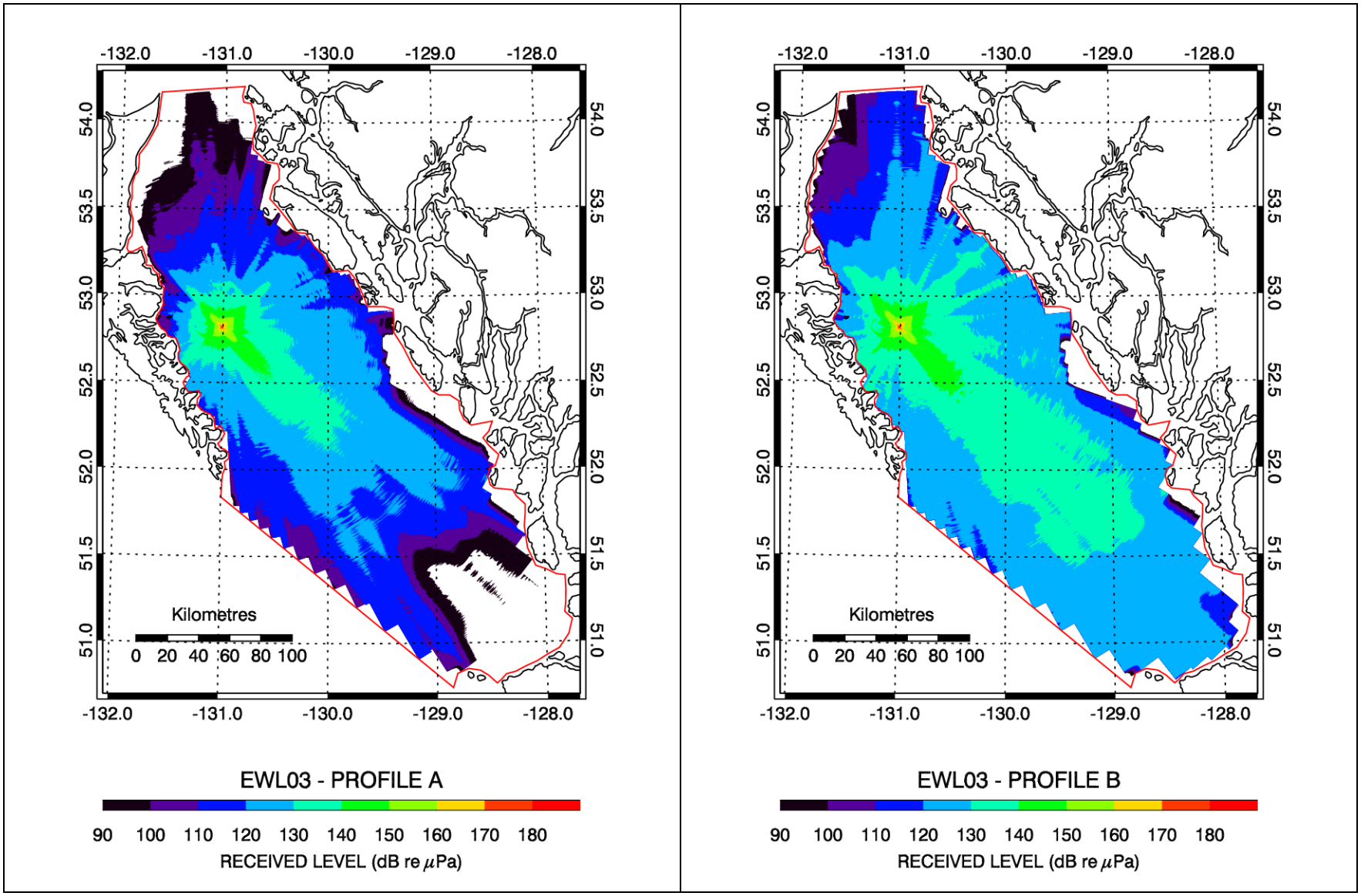
-132.0
-131.0
-130.0
-129.0
-128.0
54.0
53.5
53.0
52.5
52.0
51.5
51.0
Kilometres
0 20 40 60 80 100
EWL03 - PROFILE A
EWL03 - PROFILE B
90 100 110 120 130 140 150 160 170 180
RECEIVED LEVEL (dB re μPa)

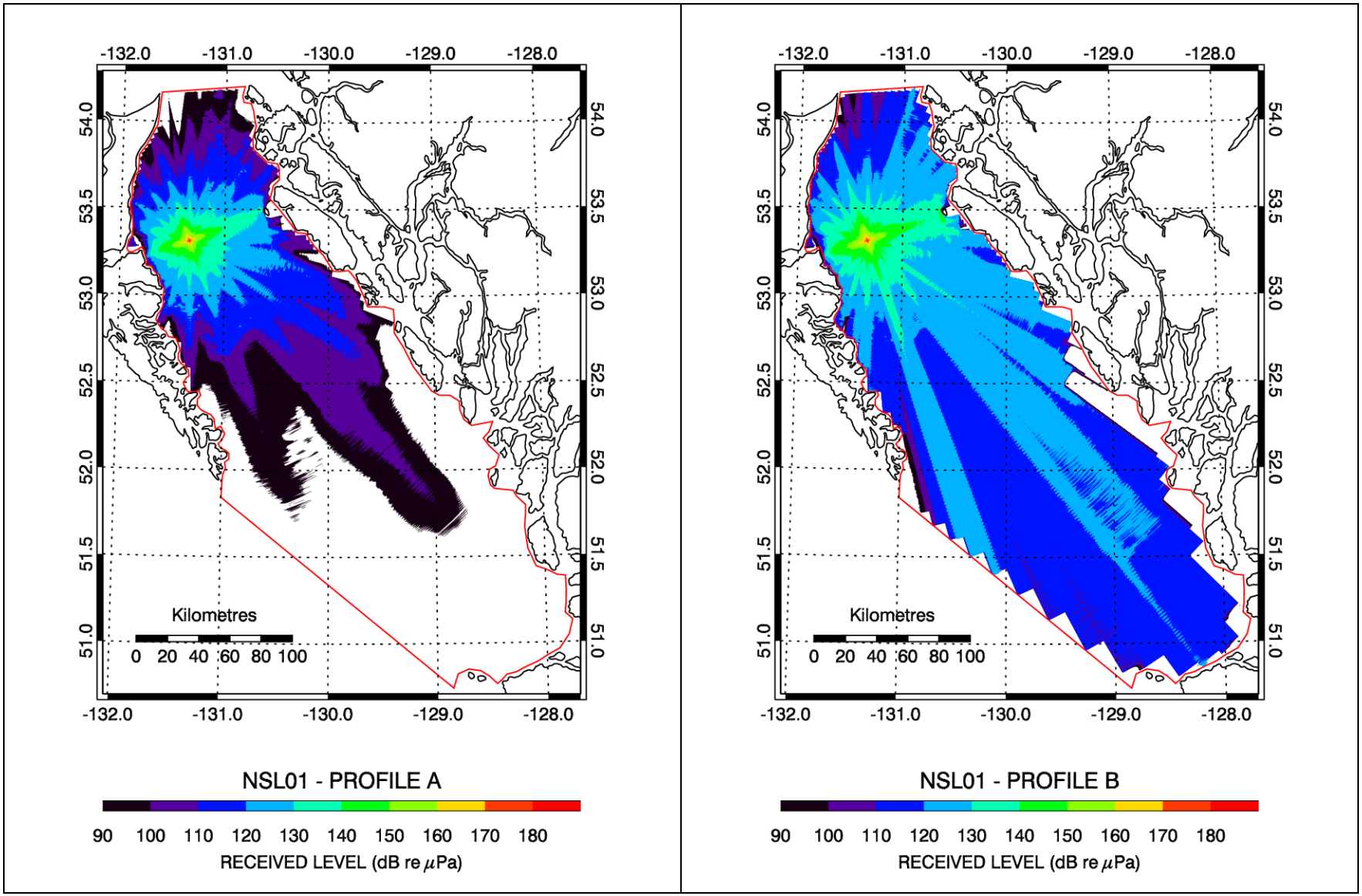
-132.0
-131.0
-130.0
-129.0
-128.0
54.0
53.5
53.0
52.5
52.0
51.5
51.0
Kilometres
0 20 40 60 80 100
NSL01 - PROFILE A
90 100 110 120 130 140 150 160 170 180
RECEIVED LEVEL (dB re μPa)
NSL01 - PROFILE B
90 100 110 120 130 140 150 160 170 180
RECEIVED LEVEL (dB re μPa)

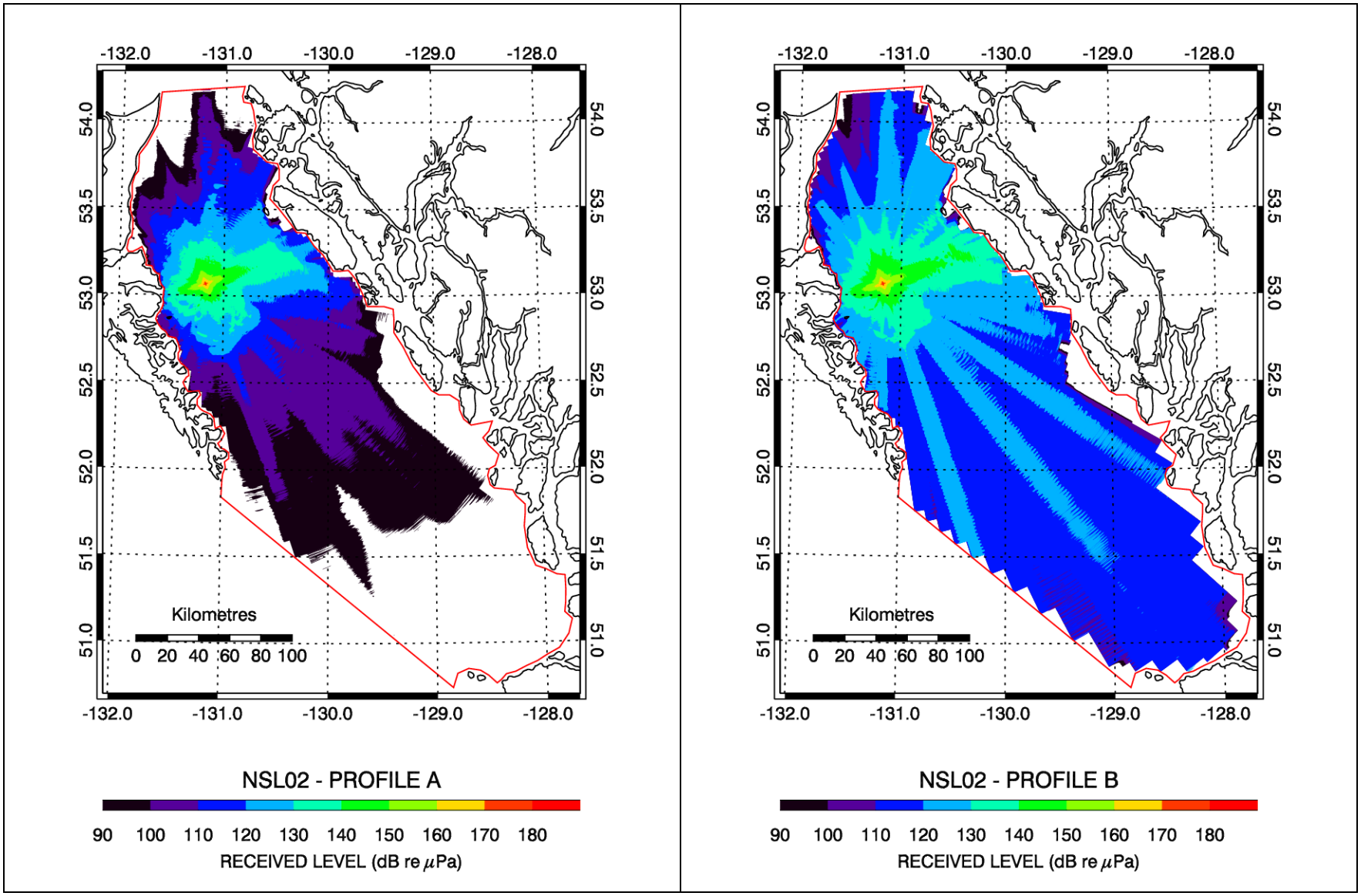
-132.0
-131.0
-130.0
-129.0
-128.0
54.0
53.5
53.0
52.5
52.0
51.5
51.0
Kilometres
0 20 40 60 80 100
NSL02 - PROFILE A
90 100 110 120 130 140 150 160 170 180
RECEIVED LEVEL (dB re μPa)
NSL02 - PROFILE B
90 100 110 120 130 140 150 160 170 180
RECEIVED LEVEL (dB re μPa)

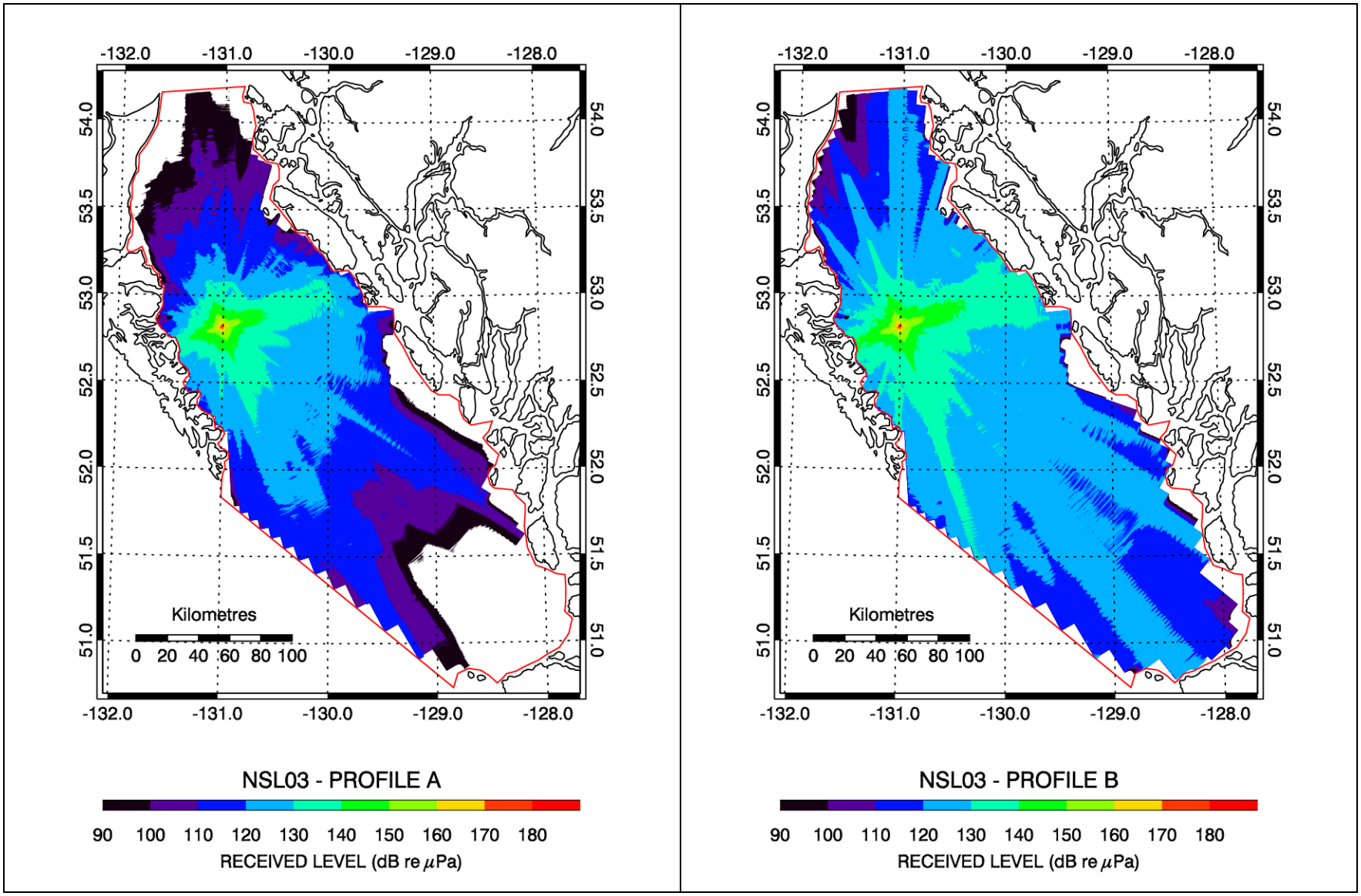
-132.0
-131.0
-130.0
-129.0
-128.0
54.0
53.5
53.0
52.5
52.0
51.5
51.0
Kilometres
0 20 40 60 80 100
NSL03 - PROFILE A
NSL03 - PROFILE B
90 100 110 120 130 140 150 160 170 180
RECEIVED LEVEL (dB re μPa)

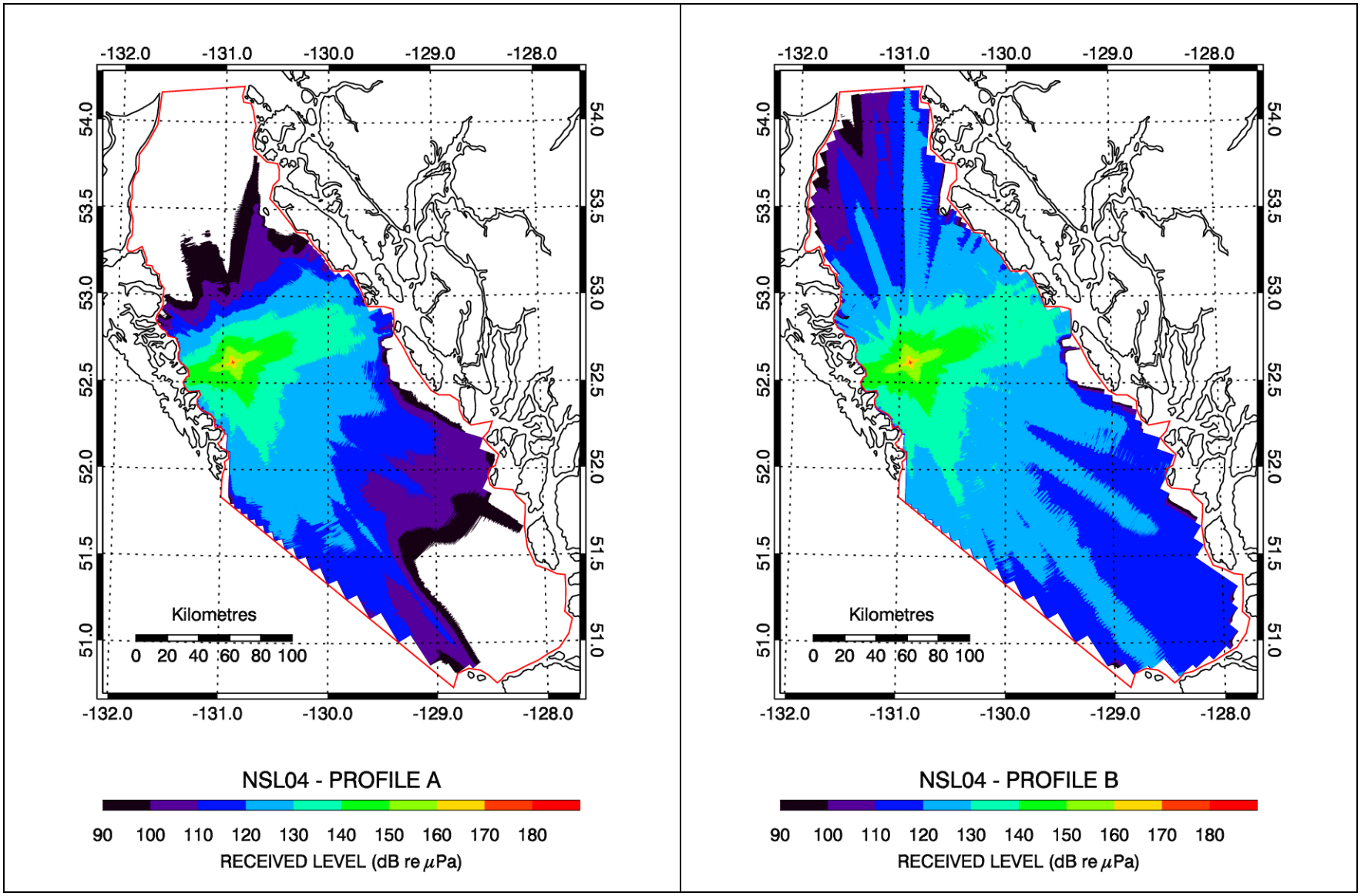
-132.0
-131.0
-130.0
-129.0
-128.0
54.0
53.5
53.0
52.5
52.0
51.5
51.0
Kilometres
0 20 40 60 80 100
NSL04 - PROFILE A
NSL04 - PROFILE B
90 100 110 120 130 140 150 160 170 180
RECEIVED LEVEL (dB re μPa)

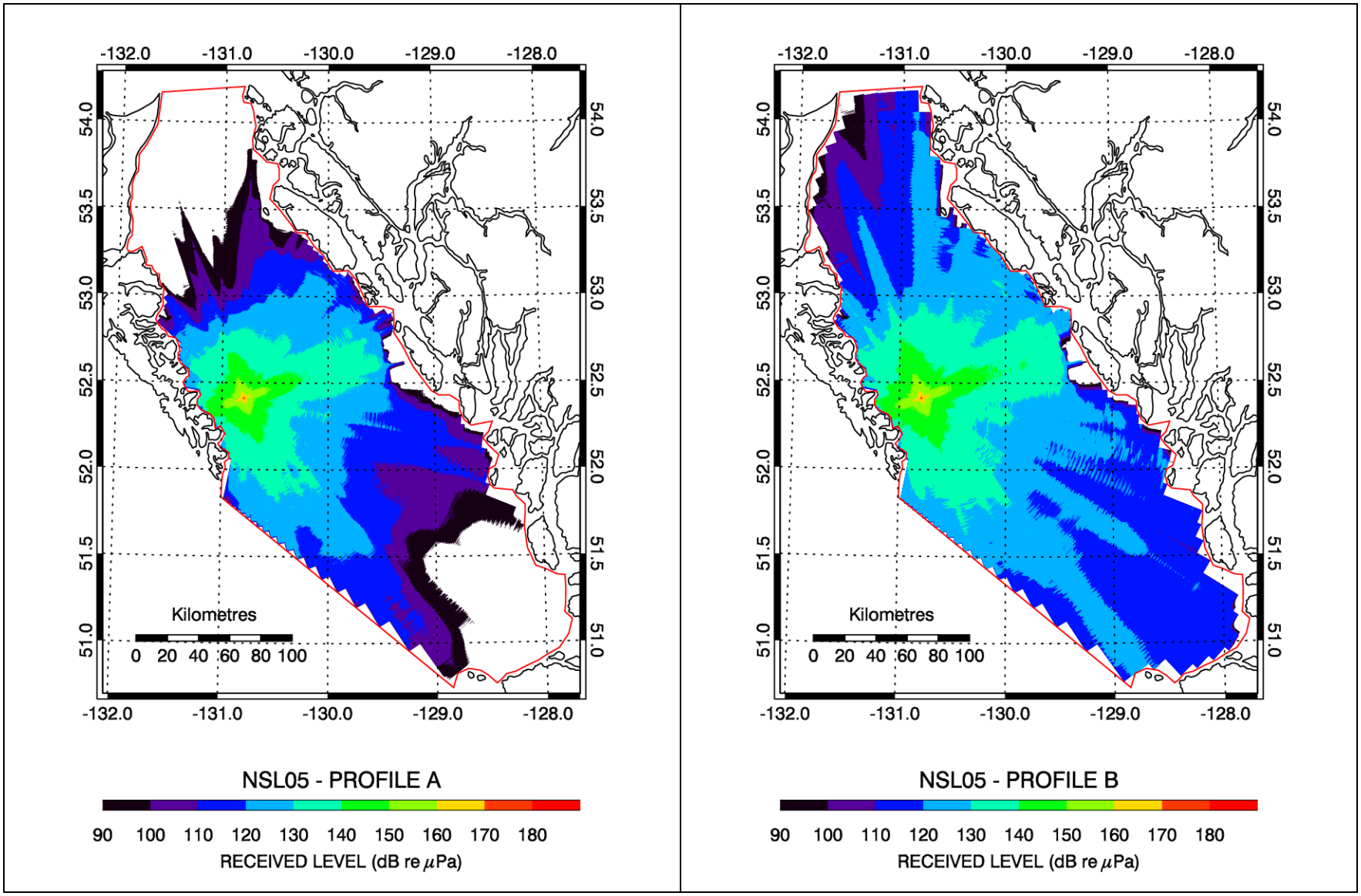
-132.0
-131.0
-130.0
-129.0
-128.0
54.0
53.5
53.0
52.5
52.0
51.5
51.0
Kilometres
0 20 40 60 80 100
NSL05 - PROFILE A
NSL05 - PROFILE B
90 100 110 120 130 140 150 160 170 180
RECEIVED LEVEL (dB re μPa)

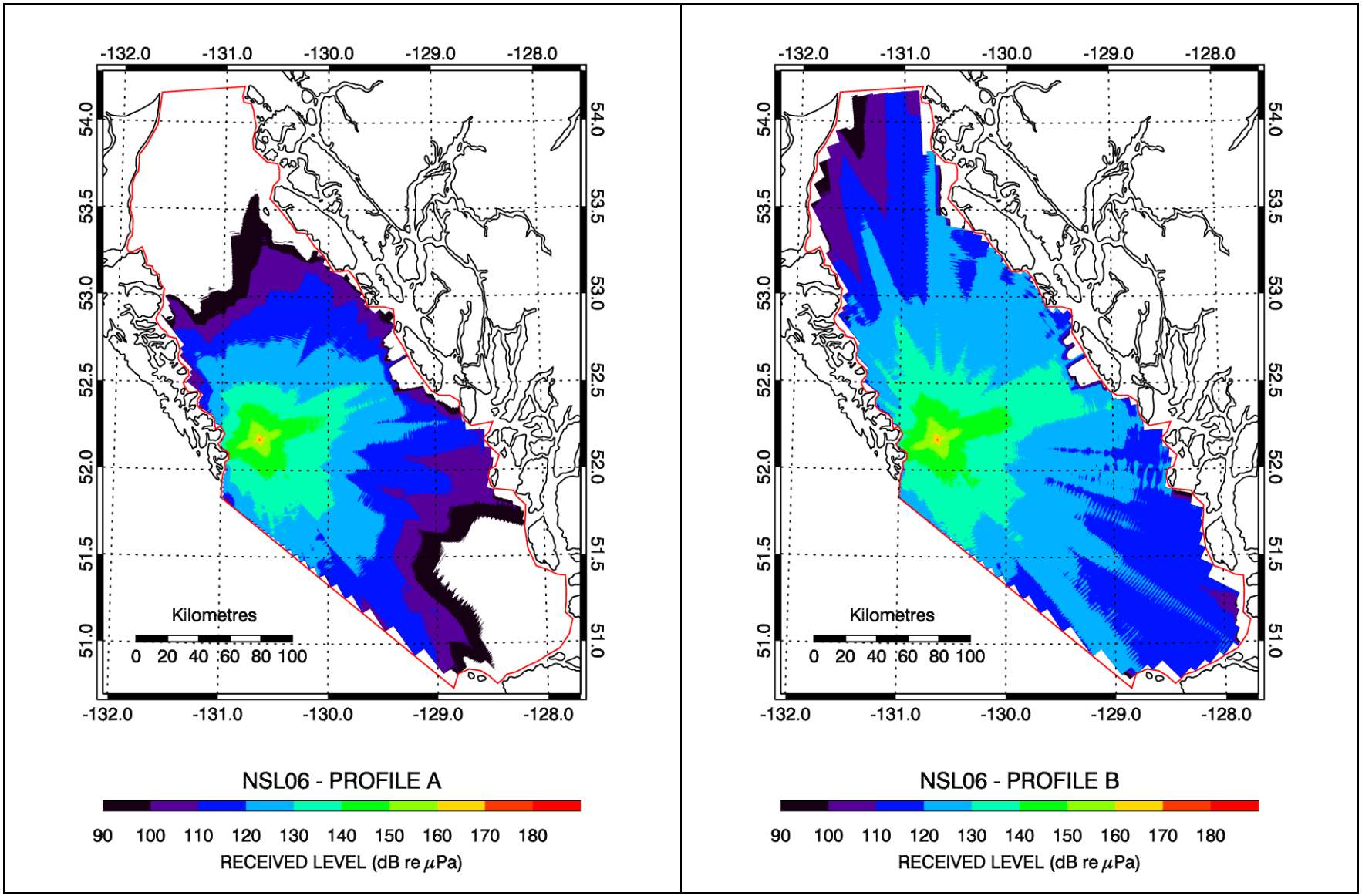
-132.0
-131.0
-130.0
-129.0
-128.0
54.0
53.5
53.0
52.5
52.0
51.5
51.0
Kilometres
0 20 40 60 80 100
NSL06 - PROFILE A
NSL06 - PROFILE B
90 100 110 120 130 140 150 160 170 180
RECEIVED LEVEL (dB re μPa)